

See discussions, stats, and author profiles for this publication at: <https://www.researchgate.net/publication/360829699>

Impact of land cover transformation on urban heat islands in Harbin, China

Article in Environmental Monitoring and Assessment · June 2022

DOI: 10.1007/s10661-022-10066-z

CITATIONS

9

READS

414

9 authors, including:



Stephen Dauda Yabo

Ahmadu Bello University

22 PUBLICATIONS 177 CITATIONS

[SEE PROFILE](#)



Dong-Lei Fu

Harbin Institute of Technology

34 PUBLICATIONS 468 CITATIONS

[SEE PROFILE](#)



Bo Li

Harbin Institute of Technology

41 PUBLICATIONS 790 CITATIONS

[SEE PROFILE](#)



Xiaofei Shi

18 PUBLICATIONS 177 CITATIONS

[SEE PROFILE](#)



Impact of land cover transformation on urban heat islands in Harbin, China

Stephen Dauda Yabo · Donglei Fu · Bo Li ·
Xiaofei Shi · Samit Thapa · Xie Shengjin · Lu Lu ·
Hong Qi · Wei Zhang

Received: 28 October 2021 / Accepted: 21 April 2022
© The Author(s), under exclusive licence to Springer Nature Switzerland AG 2022

Abstract At the local and regional climate scale, one of the most studied environmental issues is urban heat island (UHI). UHI is a thermal anomaly caused by temperature differences between urban and rural settings, which adds heat to the atmosphere and makes people feel uncomfortable. This study explores the influence of new land-cover data on UHI simulations using the high-resolution Weather

Research and Forecasting (WRF) model coupled with the single-layer urban canopy model (SLUCM) in the city of Harbin. A comparison was performed between the new Tsinghua University (TU) land cover dataset with the default United States Geological Survey (USGS) and Moderate Resolution Imaging Spectroradiometer (MODIS) land cover datasets. The results of this study revealed that the new TU land cover data had better representation and more realistic land cover changes than the default datasets. The diurnal, seasonal, and long-term nighttime UHIs

Supplementary information The online version contains supplementary material available at <https://doi.org/10.1007/s10661-022-10066-z>.

Highlights

- The new TU land cover dataset provided a better representation and more realistic land cover changes than the default datasets in the WRF.
- The high-resolution WRF/SLUCM model investigated UHI at high spatial and temporal resolution.
- The diurnal, seasonal, and long-term nighttime UHIs for T_{SK} and T_{2m} were higher than the daytime with a typical cold island in winter.
- Rapid changes in land cover revealed an increase in UHIs of satellite towns.

S. D. Yabo · D. Fu · B. Li · X. Shi · S. Thapa ·
X. Shengjin · L. Lu · H. Qi
State Key Laboratory of Urban Water Resource
and Environment, Harbin Institute of Technology, Harbin,
China
e-mail: hongqi@hit.edu.cn

S. D. Yabo · D. Fu · B. Li · X. Shi · S. Thapa ·
X. Shengjin · L. Lu · H. Qi
School of Environment, Harbin Institute of Technology,
Harbin, China

S. D. Yabo · D. Fu · B. Li · X. Shi · S. Thapa ·
X. Shengjin · L. Lu · H. Qi
Heilongjiang Provincial Key Laboratory of Polar
Environment and Ecosystem, Harbin, China

S. D. Yabo
Department of Geomatics, Ahmadu Bello University,
Zaria, Nigeria

X. Shi
CASIC Intelligence Industry Development Co., Ltd,
Beijing, China

W. Zhang
School of Computer Science and Technology, Harbin
Institute of Technology, Harbin, China
e-mail: weizhang@hit.edu.cn

of air and surface temperatures were higher than the daytime UHIs for both downtown Harbin and the satellite towns. We discovered that coal-burning during winter had a significant influence on UHI in Harbin. Moreover, the results from our buffer revealed a rapid increase in the UHIs of satellite towns, thus revealing the need to focus on the effects of UHI in satellite towns in the future. Therefore, the timely updating of land cover datasets in the WRF model and implementing mitigation strategies will help improve the urban climatic comfort.

Keywords Land-cover changes · Surface energy fluxes · Urban heat islands · Weather research and forecasting model · Single-layer urban canopy model

Introduction

The impact of global warming and the establishment of heat islands in cities is a topic that has gotten a lot of attention recently despite being in existence over the years. As the climate of cities changes due to human activities and rapid development, this has piqued international organizations' interest, encouraging them to conduct research. Based on these findings, it was predicted that when temperatures rise, mortality rates will rise between 2.2% and 32% (Cetin, 2020a, b). Climate and air have a significant effect on people's physiological and behavioral status, making human performance and climate comfort affected by climate change. Climate is the most important aspect that defines a lifestyle, and it is one of the essential components that must be taken into account in constructing structures within an ecological environment. It has been observed from pieces of literature that accelerated urbanization and global warming are factors underlying the great conurbations and land-use changes in many cities of the world (He et al., 2020; Javadinejad et al., 2021; Liu et al., 2017; Massad et al., 2019; Talebmorad et al., 2021; Zhang et al., 2020), and they have resulted in urban heat island (UHI) phenomenon, in which the temperatures of urban areas are considerably higher than those of suburban or rural regions (Oke, 1995; Zhao et al., 2017). This phenomenon is ubiquitous because it is found in cities of all climatic regions, including cities in high-altitude regions or with colder seasons (for example, Harbin, in Northeast China). The rapid changes in the built environment where green

surfaces are turned into urban areas generate or absorb more heat. Moreover, in high-density built-up areas, the temperature is discovered to be significantly higher than that in rural areas, open green areas, and forest areas (Bozdogan Sert et al., 2021; Cetin, 2019, 2020a, b; Cetin et al., 2019; Zeren Cetin & Sevik, 2020; Zeren Cetin et al., 2020). As the urban heat island rises, it adds significantly to climate warming and intense heat waves (Huang & Lu, 2015; Neethu & Ramesh, 2022; Tewari et al., 2019; Wang & Li, 2021; Zhou & Shepherd, 2010) and negatively impacts air quality, loss of biological control, water resources, urban thermal environment, increases energy consumption, outdoor thermal comfort, and human health and wellbeing (Adiguzel et al., 2022; Cetin, 2015, 2016; Cetin et al., 2018, 2019; Liu et al., 2020; Ostad-Ali-Askar et al., 2018; Talebmorad et al., 2021; Zhao et al., 2017). UHIs affect the quality of life and the livability of cities (Adiguzel et al., 2020; Cetin, 2019, 2020a, b; Zeren Cetin & Sevik, 2020; Zeren Cetin et al., 2020). Moreover, UHIs reduce energy use for heating (Oke, 1995; Yang et al., 2017a, b). Continuous growth within urban areas resulting in conurbations will lead to significant increases in UHIs (Rizwan et al., 2008), which raises great concern about future exposure to hazards caused by local warming under global climate change caused by greenhouse gas emissions and the generation of severe UHIs as a result of urban expansion (Georgescu, 2015; Palou & Mahalov, 2019; Salamanca et al., 2015; Tewari et al., 2017). Therefore, having accurate information on the UHI's effects on the environment will provide insight into the studies of bioclimatic comfort.

A study on UHI highlighted the stresses from extreme heat or cold which have the tendency to alter a person's energy balance (Cetin et al., 2018). Extreme weather phenomena or events have a wide range of implications for regional areas, particularly cities (such as Harbin). Urban cities are the hubs of human activity, and the number of people and assets at risk from extreme weather events is high, especially given the current climate. Extreme weather has always had and will continue to have substantial consequences for communities. Extreme weather events are exacerbated by climatic circumstances, which are influenced by anthropogenic climate change elements (Cetin et al., 2018). Though studies on bioclimatic structure have been well investigated and should be taken into account when designing comfortable spaces using an important biometeorological

indicator known as the Physiologically Equivalent Temperature (PET) (Adiguzel et al., 2020, 2022; Bozdogan Sert et al., 2021; Cetin et al., 2018, 2019; Cetin, 2015, 2019, 2020a; Gungor et al., 2021; Zeren Cetin & Sevik, 2020; Zeren Cetin et al., 2020). Moreover, the effect of UHI has a strong connection with extreme heat/cold which in turn exerts significant consequences on cities with these extreme climates. It is worthy to note that this study examined the two extreme seasons (summer and winter) in order to provide a basis for future studies on bioclimatic comfort. However, the accurate forecasting of urban climate UHIs are gaining more importance; hence, high-resolution simulation models have become necessary to depict the extent of the impact of UHI within the study area.

The most often utilized methodologies for studying UHI include in-situ observation, remote sensing observation, and numerical modeling (Holec et al., 2020; Huidong, 2018; Li et al., 2019, 2018a, b; Mirzaei & Haghishat, 2010; Tewari et al., 2019; Porangaba et al., 2021). In most cases, in-situ observations have a limitation of being unable to accurately depict the spatial pattern of UHI due to the limited number of stations, while remote sensing observations are limited in capturing accurately the temporal variations of UHI due to low temporal resolution and cloud disruptions. In contrast to in-situ and remote sensing observations, numerical modeling can be used to investigate UHI at high spatial and temporal resolution (José et al., 2013). Numerical modeling is an effective approach that has a wide range of successful applications that have been reported by Huidong (2018). The use of numerical models for applied science computations enhances the results for the present and future climate of cities, as suggested by Myrup (1969). In the twenty-first century, the Weather Research and Forecasting (WRF) model, coupled with the land surface model (LSM), started gaining ground in the study of UHIs (Chen et al., 2004, 2011a, b). Moreover, several recent studies utilized the coupled Weather Research and Forecasting/Urban Canopy Model (WRF/UCM) to assess UHIs, urban morphology, and aerosol effects (Bhati & Mohan, 2016; Zhong et al., 2017; Zhou & Chen, 2018; Ghadban et al., 2020; Holec et al., 2020; Jandaghian & Berardi, 2020). The single-layer urban canopy model (SLUCM) was used in various studies (Giannaros et al., 2013, 2018; Yang et al., 2012) and recently in the study of heat stress and UHI under calm and fair conditions in China, heatwaves in

Boston and Phoenix, and sensitivity dense advection fog events in Istanbul, Turkey (Neethu & Ramesh, 2022; Wang et al., 2020; Wang & Li, 2021; Zhang et al., 2020). The significance of using the SLUCM is that it depicts the dynamics of urban surface heat fluxes (Chen et al., 2011a, b; Tewari et al., 2019), improves the description of lower boundary conditions, and produces more accurate forecasts for metropolitan areas (José et al., 2013). However, this method still suffers from the inadequate specification of land cover data, which is a basic problem in numerical simulations (Oke, 1988; Rizwan et al., 2008; Sertel et al., 2010; Cheng et al., 2013; Li et al., 2018a, b); thus, more specific data are required for the modeling of temperature-related UHIs. Therefore, this study highlighted the need for a high-resolution model as a basis for the studies of urban heat islands and the need for timely updating of the land cover dataset in the model so that the UHI effect can be depicted and provide a basis for research studies on climate comfort in this region.

In urban climate modeling, the land cover dataset influences the simulation of land surface processes, which play a major role in land-use/land-cover changes and their biogeophysical and biogeochemical effects on the climate system (Brovkin et al., 2013; Friedl et al., 2002; Mahmood et al., 2014) in both regional and mesoscale and large-scale atmospheric models (Chen & Dudhia, 2001). The surface-atmosphere fluxes of sensible heat, latent heat, and their momentums are influenced by variations in physical features of the land surface from land cover data, which in turn influence weather and climate (Sellers et al., 1997). The default land cover data prescribed in the WRF model are unsatisfactory and do not give a proper representation in line with current urban surface features (Li et al., 2018a, b). Mirzaei and Haghishat (2010) highlighted that land-use land cover is a major limitation in urban canopy models. Therefore, to depict the characteristics of the real surface, it is essential to update land cover data constantly. Recently, Li et al. (2018a, b) found that current Urban Atlas and CORINE land cover data (covering only Europe) were able to represent both land surface and air temperatures in Berlin than USGS data; however, these datasets lack global coverage. To date, there is a lack of an updated land cover dataset in the WRF model in order to estimate the current urban surface features as a result of rapid development. It is on this note that studies across the world that adopted the WRF model find it necessary to incorporate any new

dataset into the model in order to achieve their desired results. The temporal and spatial variations between the default datasets and the new dataset also the variations between urban and rural areas are the main causal factors triggering UHIs (Rizwan et al., 2008). Consequently, continuous updates of land cover data are required to provide accurate inputs for modeling runs. Hence, to the best of our knowledge, the latest Tsinghua University land cover dataset (TU_LC, 2017) with high resolution and good representativeness was incorporated into the WRF model which has never been used in the study of UHI. Therefore, this provided a basis of comparison with the default datasets derived from USGS (~1 km, 1994) and MODIS data (~resolution, 2005) for the purpose of examining the long-term effect of UHI in the city of Harbin and its environs.

This paper focuses on the city of Harbin and its satellite towns located in Northeast China. Harbin is the main industrial base of China and has witnessed drastic transformation due to rapid development in recent years (Xiaolin, 2017). Recent studies on land-use changes in Harbin revealed that construction land contributed significantly to generating impervious surfaces, which in turn increased the temperature within the urban/suburban settings compared to the rural counterparts (Jihong et al., 2020; Xiaolin, 2017; Zhao et al., 2015). Moreover, Harbin and the surrounding satellite towns frequently witnessed severe pollution effects due to the very long coal heating season (six months, from October to April the following year). Due to adverse meteorological conditions and intense emissions during the heating season, severe pollution episodes have threatened public health in the region and influenced climate change (Sun et al., 2020). The land-use and land cover transformation induced UHIs spanning for 25 years over Harbin; hence, determining the performance and advantages of the new dataset alongside the default datasets (MODIS and USGS) with updated anthropogenic heat (AH) in the WRF/SLCUM modeling runs is the first objective of this paper. This study also investigates the significance of the updated dataset on the surface energy fluxes related to the enhancement in temperature. Consequently, we examined the spatial influence of land cover on temperatures across summer and winter to gain insight into the study of urban heat islands and cold islands in the coldest megacity in China. Finally, we investigated the performance of

satellite towns concurrently with downtown towns to have insights into the effects of UHI on these potential upcoming cities (referred to as satellites) in order to provide the necessary information needed for effective planning of bioclimate comfort in the city and its environs. Moreover, the impact exerted by the land cover on UHIs indicates that the influence of UHIs on air pollution should be investigated based on the emission reduction policy promulgated in Harbin in 2016.

Materials and methods

Study area

Harbin is situated at longitude 125.4–130.1° E and latitude 44.0–46.4° N. It is the provincial capital of Heilongjiang Province as well as the Northeast China Plain's most advanced industrial and agricultural megacity, and it has the largest land area of 10,200 km². Among all provincial capitals in China, it ranks as the third-largest with a registered population of 5.5 million (Chen et al., 2018). Harbin's climate is generally continental monsoon, with a long winter that lasts for more than 5 months with snow cover lasting from November to March and lowest temperatures occurring in January (−37.7 °C), and a short summer season from June to August with an average temperature of 23 °C. The average annual precipitation is 569.1 mm. The region's topography can be categorized as a typical valley landform with a mean elevation of 136 m. The XiaoXing'an Mountains run through the northern part of Harbin, while the offshoot hill of Zhangguangcai Ridge runs through the southern part. Harbin's urban area is primarily distributed along with the three-ladder formation of the Songhua River, which passes through the city's center (see Fig. 1b). The area surrounding Harbin has been actively cultivated over the last 50 years. The Northeast China Plain has developed into one of China's key agricultural areas (Wang et al., 2011; Zhao et al., 2015; Huang et al., 2018; Sun et al., 2020). Moreover, land cover changes in Harbin have been prevalent since 2000 due to growing industrialization and urbanization changes, particularly in the urban area and its environment, where farmland and forest land cover categories have been reclassified as urban and built-up land. As a result of these

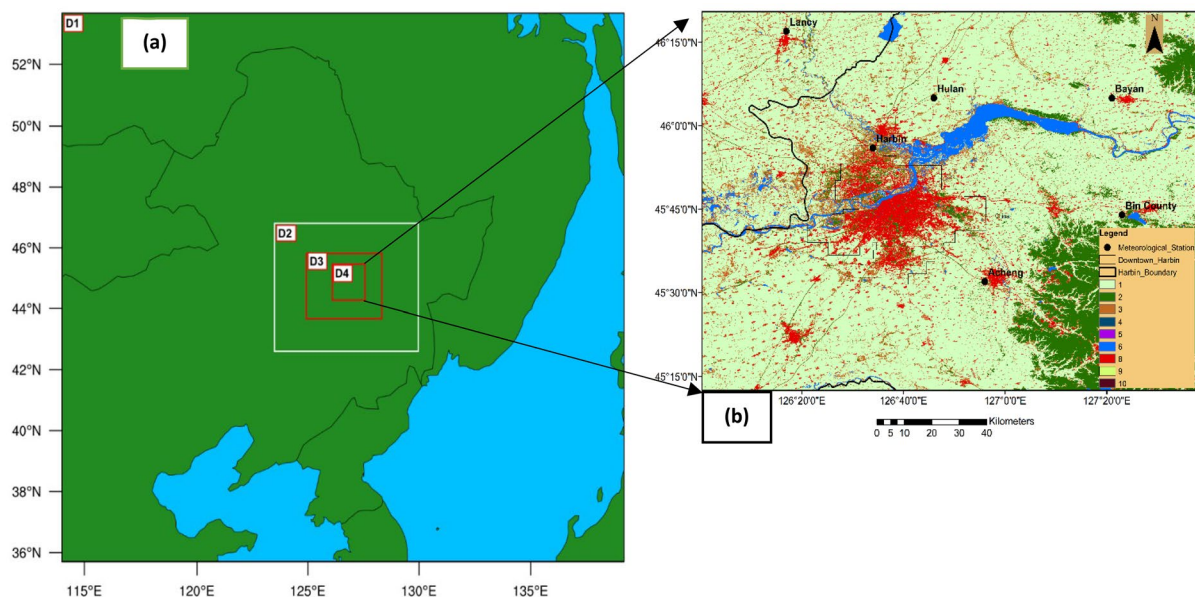


Fig. 1 (a) Domains in this study with horizontal spatial resolutions of 27 km (D1), 9 km (D2), and 3 km (D3) and the focused innermost domain (D4) and (b) TU land cover of the innermost domain (Harbin) with a resolution of 1 km. Note:

1_Farmland, 2_Forest, 3_Grassland, 4_Shrub, 5_Wetlands, 6_Water body, 7_Tundra, 8_Impervious layer, 9_Bare ground, 10_Ice and snow

changes, impervious surfaces have been generated within the city, thereby enhancing the effect of urban heat islands. Consequently, in order to prevent straw accumulation, agricultural waste is frequently burned in the area, resulting in enormous levels of air pollution with severe effects on human health in the region (Cao et al., 2016). These continuous haze events are being contested for some years now with an emphasis on the necessity for rigorous emission reduction (Fu et al., 2021a, b).

Data used

Land cover data is one of the major datasets used to drive the WRF-SLUCM model. The model incorporates default land cover datasets developed by the US Geological Survey and retrieved from the 1-km Advanced Very High-Resolution Radiometer (AVHRR) satellite from April 1992 to March 1993 (Loveland et al., 1995), and they were chosen to account for changes in the 1990s. The USGS has a 49% precision increment; hence, it was chosen as the earliest dataset in the WRF (Gong, 2009). The second default dataset used was the MODIS IGBP which was derived from MODIS satellite data collected from

2001 to 2005 (Friedl et al., 2002). The MODIS data was chosen to account for the changes in the 2000s, and it had a global accuracy of 72.3% and 77.4% (Friedl et al., 2010). Hence, across China, the accuracy ranges from 31.86 to 58.65% (Yang et al., 2017a, b). These default land cover datasets prescribed in the WRF model do not give a proper representation in line with current urban surface features (Li et al., 2018a, b); hence, they are unsatisfactory to address the effect of UHI. Therefore, in order to address the limitation of the land cover dataset in the WRF model highlighted by Mirzaei and Haghhighat (2010), the new Tsinghua University land cover (TU_LC) dataset was incorporated into the model to depict the current state of the effect of UHI in the city of Harbin.

The new TU_LC dataset was retrieved from MOD13Q and Landsat 8 by the Department of Earth System Science in 2017 at an approximately 30 m resolution, and it has a classification accuracy of 72.35% (Fig. 1b). The TU_LC has been chosen to account for the changes in the 2010s; hence, its accuracy increases by 4.65~36.85% compared with the normally used datasets (e.g., GLC2000, CCI-LC 2010) (Yang et al., 2017a, b). Consequently, because of its high spatiotemporal resolution relative to the

default dataset, it is suitable to depict the current transformation of the simulated urban temperature. Moreover, the urban/built-up category classified in the USGS land cover dataset was reclassified into low-intensity residential, high-intensity residential, and industrial/commercial in the UCM using the mosaic approach (with tile number $N=3$) in previous studies (Fu et al., 2021a, b; Li et al., 2013; Li & Bou-Zeid, 2014). It was found to be a suitable method for reclassification of the new dataset in order to efficiently maintain the sub-grid influence in the WRF-SLUCM model. We used the mean values of the anthropogenic heat in the SLUCM that corresponded to the three reclassified urban categories as follows: commercial/industrial (93.0), high-density residential (65.0), and low-density residential (27.0) based on actual conditions (<http://tjj.jl.gov.cn/tjsj/tjnjl/>; <http://www.hlj.gov.cn/zwfb/zfcbw/hljtnjl/>).

The second most important dataset used to drive the WRF model is the Global Final Analysis (FNL) retrieved from the National Center for Environmental Prediction (NCEP). It is used for the initial and lateral boundary conditions in the WRF model, and they have a horizontal resolution of 1° by 1° at 6-h intervals (<ftp://nomads.ncdc.noaa.gov/GFS/>). The details of how the data are being run by the WRF Preprocessing System (WPS) can be found in the WRF manual (<http://www2.mmm.ucar.edu/wrf/users/>).

Additionally, the hourly observation weather station data were collected from the China Meteorological Data Service Center (<http://data.cma.cn/>). These data were necessary for the evaluation of the model simulation of the 2-m air temperature (hereafter referred to as T_{2m}). Similarly, land surface temperature (LST) data obtained from MODIS satellite observations (version 6, level 3) was used for the purpose of validating the surface skin temperature (hereafter

referred to as T_{SK}). The daily MYD11A1 LST was observed by the AQUA satellite at 1:30 pm (UTC) on August 2, 2019, and December 17, 2019, and these days were chosen due to the limited cloud cover at the time of acquisition (<https://ladsweb.modaps.eosdis.nasa.gov/search/>). The LST images were reprojected and resampled with the model grids in the innermost domain using ArcGIS desktop 10.5. The processed data can be seen in Supplementary Figs. S3 and S4 for both summer and winter, respectively.

In this study, three land cover datasets were used to design the experiments (refer to Table 1). Three simulations for each season (summer and winter) were planned via diverse configurations and information on land cover data based on measurement stations, as presented in Table 2. As shown in Table 1, four domains (here referred to as Dom_1, Dom_2, Dom_3, and Dom_4) were designed for the entire experiment. The first experiment was designed using the USGS land cover (USGS_LC) default data across the four domains. The USGS_LC data had 141 urban grids accounting for 8.84% in Dom_4. The MODIS_LC default dataset was used in the second experiment to account for 19.62% of the 313 urban grids. The MODIS_LC was employed in all the domains. The third experiment was designed using the new TU_LC data in Dom_2, Dom_3, and Dom_4 while the USGS_LC was used in Dom_1. The reason is that the new dataset had a coverage limited to Northeast China and its environs. The TU_LC dataset had the largest urban grid of 1141, accounting for 71.54% in the Dom_4. The urban grids showed the urban spatial extent as a result of urban expansion. Moreover, the land cover categorization shown in Table 2 depicts the dominant land cover type in downtown Harbin and the four satellite towns for TU_LC, MODIS_LC,

Table 1 Land cover configuration of the data for the three simulations for the urban land category within domain 4

Simulations	Land cover data configuration					
	Dom_1	Dom_2	Dom_3	Dom_4	No. of urban grids	Urban grids (%)
USGS_LC (Default)	USGS	USGS	USGS	USGS	141	8.84
MODIS_LC (Default)	MODIS	MODIS	MODIS	MODIS	313	19.62
TU_LC (New)	USGS	TU_LC	TU_LC	TU_LC	1141	71.54

USGS_LC, MODIS_LC, and TU_LC represent US Geological Survey Land Cover, Moderate Resolution Imaging Spectroradiometer Land Cover, and Tsinghua University Land Cover, respectively. Dom_1, Dom_2, Dom_3, and Dom_4 represent domains 1, 2, 3 and 4, respectively

Table 2 Land cover information at observation stations

Station (s)	LON (E)/LAT (N)	Category	USGS	MODIS	TU
			Dominant LC	Dominant LC	Dominant LC
Acheng	126.93/45.53	Satellite Town (ST)	Cropland/Pasture	Cropland	Cropland/Built-up
Bayan	127.35/46.08	Satellite Town (ST)	Cropland/Pasture	Cropland	Cropland
Binxian	127.38/45.73	Satellite Town (ST)	Cropland/Pasture	Cropland	Cropland
Harbin	126.57/45.93	Downtown (DT)	Urban/Built-up	Urban/Built-up	Urban/Built-up
Hulan	126.76/46.08	Satellite Town (ST)	Cropland/Pasture	Cropland	Cropland/Built-up

LON and LAT represent longitude and latitude. LC represents land cover. E, N represents eastings and northings

and USGS_LC datasets. The built-up land category primarily dominates downtown Harbin (DT), and the cropland/built-up primarily dominates the satellite towns (Acheng, Hulan, Binxian, and Bayan) in the new TU_LC dataset, respectively.

Configuration of the WRF model

In this study, the WRF model version 4.0 was employed. This is a numerical weather forecast system created by the National Center for Atmospheric Research in the USA. In order to solve urban environmental issues, this study used an integrated urban modeling system in conjunction with WRF's Noah LSM scheme. The UCM utilized in this work is an SLUCM that considers anthropogenic heat sources, shadowing, reflections, radiation trapping, street orientation, diurnal azimuth angle change, surface energy budget of roofs, walls, roadways, and wind profile in the canopy layer (Kusaka et al., 2005; Li et al., 2019). The SLUCM (applied in the innermost domain), the mosaic approach, and updated anthropogenic heat data were incorporated into the WRF model for the purpose of addressing the effect of UHI in the city of Harbin. The coupled model's major goal is to improve the description of lower boundary conditions, depict the dynamics of urban surface heat fluxes, and produce more accurate forecasts for metropolitan areas (Chen et al., 2011a, b; José et al., 2013; Tewari et al., 2019). Four domains were designed with horizontal grid spacings of 27 km (D1), 9 km (D2), 3 km (D3), and 1 km (D4), with the innermost domain (D4) covering the Harbin metropolis and its environs (Fig. 1a). The simulations were carried out from July 15 to August 15, 2019, and from December 15, 2019, to January 15, 2020, for summer and winter, respectively. These periods are considered the peak for both

summer and winter with the possibility of extreme heat and cold. The first 48 h were used to initialize the system and were not included in the computation and evaluation of the results. Domain 4 (finest) simulation results were utilized to evaluate and research the characteristics of UHI in Harbin. The physical parameterization schemes selected for this simulation were as follows: (1) the Noah LSM land surface process scheme, (2) the WRF Single Moment Five-Class (WSM5) micro-physics scheme, (3) the Mellor-Yamada-Janjic planetary boundary layer scheme, (4) the Eta surface layer similarity scheme, and (5) the Dudhia and Rapid Radiative Transfer Model (RRTM) shortwave and longwave radiation schemes, respectively (Fu et al., 2021a, b; Jain et al., 2021; Wang & Sun, 2018). The WRF model is a potential tool for studying urban climate change, and it has been widely employed in different parts of the world (e.g., Europe, Asia, USA) for a variety of applications such as thermal comfort, incorporation of an open street map (OSM) into the model, ERA-interim reanalysis data, climate warming, urban morphology, estimating of local climate zones, estimating near-surface UHI intensity, UHI under calm and fair conditions, and snowfall (Arghavani et al., 2020; Göndöcs et al., 2017; Huang & Gao, 2018; Huang & Lu, 2015; Li et al., 2020; Mughal et al., 2020; Vogel & Afshari, 2020; Wang et al., 2020; Wang & Sun, 2017).

In addition, this study compared the changes in the energy flux with changes observed in the type of surface affecting heat transfer from the surface to the atmosphere. Hence, the method by Chen et al. in the WRF model was adopted in computing the sensible heat flux is expressed in Eq. (1) as follows:

$$\text{SHF} = (1 - \alpha)S_D + \epsilon(L_D - \sigma T_{\text{sfc}}^4) - LHF + G_0 \quad (1)$$

where SHF is the sensible heat flux; S_D and L_D represent the downward shortwave and longwave radiations,

respectively; T_{sfc} represents the surface temperature; σ denotes the Stefan–Boltzmann constant; α and ε represent the surface albedo and surface emissivity, respectively; and LHF and G_0 denote the latent heat flux and soil heat flux, respectively (Chen et al., 2011a, b).

Equations (2)–(4) show the method used by Sun and Mahrt (1995) in the WRF model to calculate the surface temperature as the air temperature was heated by upward longwave radiation and convective heat from the ground. The emissivity is represented by ε , which is a critical metric that regulates the quantity of surface-to-air radiation and causes temperature fluctuations during the day and at night:

$$T_g = [(R_{lw}^{\uparrow} - (1 - \varepsilon)R_{lw}^{\downarrow})/\varepsilon\sigma]^{1/4} \quad (2)$$

where R_{lw}^{\uparrow} represents the downward longwave radiation and R_{lw}^{\downarrow} corresponds to the upward longwave radiation. In the WRF model, T_{2m} is determined using:

$$T_{2m} = T_s - \frac{H}{\rho c_p C_H} \quad (3)$$

$$C_H = \frac{k \times u_*}{\ln\left(\frac{2m}{z_{0h}}\right) - \psi_H} \quad (4)$$

where ρ and c_p are the air density and heat capacity of the air, correspondingly. The von Karman's constant, $k=0.4$, the roughness length for heat is represented by z_{0h} while the integrated universal function for heat is represented by ψ_H and u_* denotes the friction velocity at 2 m (Sun & Mahrt, 1995). Therefore, the WRF-SLUCM has been applied in this study because of its high resolution to depict urban surface heat exchange and its wide application in the field of urban climate.

Measures of evaluation

Five meteorological weather stations in downtown Harbin and its environs provide hourly ground-based observations of meteorological data (see Table 2) which were used to validate the model. The point at the downtown (DT) Harbin was used as the urban point, while the satellite towns (ST) stations were selected as the suburban points (namely, Acheng, Bayan, Binxian, Hulan). The simulated T_{2m} was evaluated using the observation data obtained from the meteorological stations mentioned

above. Meanwhile, the simulated T_{SK} was evaluated using the LST data obtained from MODIS satellite observations (version 6, level 3). The daily MYD11A1 LST was observed at 1:30 pm (UTC) by the AQUA satellite on August 2, 2019, and December 17, 2019, and these days were chosen due to the limited cloud cover (<https://ladsweb.modaps.eosdis.nasa.gov/search/>). The LST images were reprojected and resampled to fit the model grids in the innermost domain using ArcGIS desktop 10.5 software. The simulated surface skin temperature and 2 m air temperature were evaluated against observation data relative to the results obtained from the simulation of the three land cover datasets utilized in this study. The model evaluation measures were the mean bias (MB) which was used to measure the deviation when compared with observations, root mean square error (RMSE) was used to measure the standard deviation of the residuals (prediction errors), and Pearson correlation coefficient (r) was employed to measure the linear correlation between the simulated and the observed data. Microsoft Excel was used as a medium for all these computations. These measures were computed from the following Eqs. (5)–(7):

$$MB = \frac{1}{n} \sum_{i=1}^n (T_{s,i} - T_{o,i}) \quad (5)$$

$$RMSE = \sqrt{\frac{\sum_{i=1}^n (T_{s,i} - T_{o,i})^2}{n}} \quad (6)$$

$$r = \frac{1}{n-1} \sum_{i=1}^n \left(\frac{T_{s,i} - \mu_{T_s}}{\sigma_{T_s}} \right) \left(\frac{T_{o,i} - \mu_{T_o}}{\sigma_{T_o}} \right) \quad (7)$$

where $T_{o,i}$, $T_{s,i}$ represent the observed and simulated temperatures at the time i for surface skin temperature and grid i for in-situ 2 m air temperature (°C), respectively. The temperature's average and standard deviation are denoted by μ and σ , respectively. The frequency of the extracted data is denoted as n .

Furthermore, the Taylor diagram was employed to validate the performances of the model using the new dataset (TU) and default datasets (MODIS and USGS) at the five meteorological stations used in this study. A Taylor diagram is a graphical technique for evaluating the validity of models which uses Pearson's correlation (r), centered RMSE, and standard deviation (SD) statistics as the basis for measurement (Taylor, 2001). The simulation's accuracy improved as simulated

points became closer to the reference (REF) point. The details can best be seen from the results shown in Supplementary Figs. S1 and S2 for both the summer and winter seasons, respectively.

The ESRI package (ArcGIS desktop 10.5) was used to delineate a buffer at 10 km for downtown Harbin and its surroundings, while other buffers were delineated at 5 km for each of the satellite towns and the surroundings. This was done in order to extract the spatial area-averaged temperature difference between downtown core/satellite town centers and their surroundings. The purpose of these extractions was to find the area-averaged temperature difference between the urban centers and their suburban/rural counterpart, hence establishing the UHI concept. The temperatures at grid points within these buffers were extracted using the NCAR Command Language (NCL) package. The NCL is a powerful software that was used to extract the spatial maps shown in this study. The Origin Pro version 2021 was utilized for most of the linear plots.

Results

Evaluation of the simulated temperatures

The seasonal evaluations were based on the performance of the observation data from meteorological stations with the T_{2m} and the MODIS observation data with the T_{SK} . The thirty-two-day-long simulated results for both T_{2m} and T_{SK} were evaluated using observation data from meteorological stations (i.e., Acheng, Bayan, Binxian, Harbin, and Hulan) and the remote sensing MODIS dataset, respectively. The simulations were performed for thirty-two days

in both summer (mid-July to mid-August 2019) and winter (mid-December 2019 to mid-January 2020) each. It is worth noting that only thirty days were used in the analysis, with two days being discarded and considered as “spin-up” based on the model term. All simulations were based on the three land cover datasets (TU, MODIS, and USGS) used in the WRF/SLUCM model. Tables 3 and 4 showed the MB, RMSE, and r for the simulated T_{2m} validated from the observed data for both summer and winter, respectively. During the summer simulations (Table 3), the lowest RMSEs had the same values at Bayan (2.57 °C and 2.87 °C) and Hulan (2.57 °C and 2.87 °C), respectively, which accounted for the good performance of TU and USGS land cover datasets over the MODIS data. However, slightly higher RMSEs were observed for TU land cover data in the satellite towns of Acheng and Binxian and downtown Harbin compared with MODIS and USGS datasets. Additionally, the minimum mean temperature biases were observed at Hulan (0.34 °C and 0.19 °C) and Bayan (0.68 °C and 0.34 °C) for the TU and MODIS land cover datasets, respectively, while for the USGS, the minimum temperature biases were observed at Bayan (0.20 °C) and Harbin (0.36 °C). For the Pearson correlation coefficient, the strongest correlation was observed at the Hulan satellite town with 0.87 across the three land cover datasets. The lowest correlation of 0.80 was also noticed at Acheng satellite town for MODIS and USGS land cover datasets each. Further evaluation was made for the T_{2m} using the Taylor diagram, as shown in Supplementary Fig. S1. We found from the summer result that TU data performed better at the Hulan, Acheng, Bayan, and Binxian than MODIS and USGS data. The strongest correlation was observed at Hulan for TU, MODIS, and USGS datasets. It can

Table 3 Summer RMSE, MB, and r of the simulated T_{2m} compared with observation data

Station (s)	RMSE			MB			r		
	TU-OBS	MODIS-OBS	USGS-OBS	TU-OBS	MODIS-OBS	USGS-OBS	TU-OBS	MODIS-OBS	USGS-OBS
Acheng	2.87	2.67	2.68	1.48	0.46	0.55	0.83	0.80	0.80
Bayan	2.57	2.68	2.57	0.68	0.34	0.39	0.85	0.83	0.84
Binxian	3.01	2.82	2.76	1.25	0.51	0.46	0.83	0.82	0.81
Harbin	2.86	2.84	2.76	0.75	0.46	0.36	0.83	0.83	0.82
Hulan	2.87	2.90	2.87	0.34	0.19	0.20	0.87	0.87	0.87

MB, RMSE, and r correspond to mean bias, root mean square error, and correlation, respectively. OBS represents the observed value

Table 4 Winter RMSE, MB, and r of the simulated T_{2m} compared with observation data

Station (s)	RMSE			MB			r		
	TU-OBS	MODIS-OBS	USGS-OBS	TU-OBS	MODIS-OBS	USGS-OBS	TU-OBS	MODIS-OBS	USGS-OBS
Acheng	5.67	6.34	6.12	-3.55	-4.29	-3.89	0.78	0.78	0.77
Bayan	5.48	5.52	5.50	-1.80	-2.26	-1.67	0.82	0.82	0.81
Binxian	4.54	5.08	4.93	-1.53	-2.30	-1.96	0.84	0.84	0.83
Harbin	5.88	6.37	6.13	-3.38	-4.03	-3.50	0.77	0.79	0.79
Hulan	5.46	5.88	5.69	-2.11	-3.12	-2.63	0.84	0.83	0.83

MB, RMSE, and r correspond to mean bias, root means square error, and correlation, respectively. OBS represents the observed value

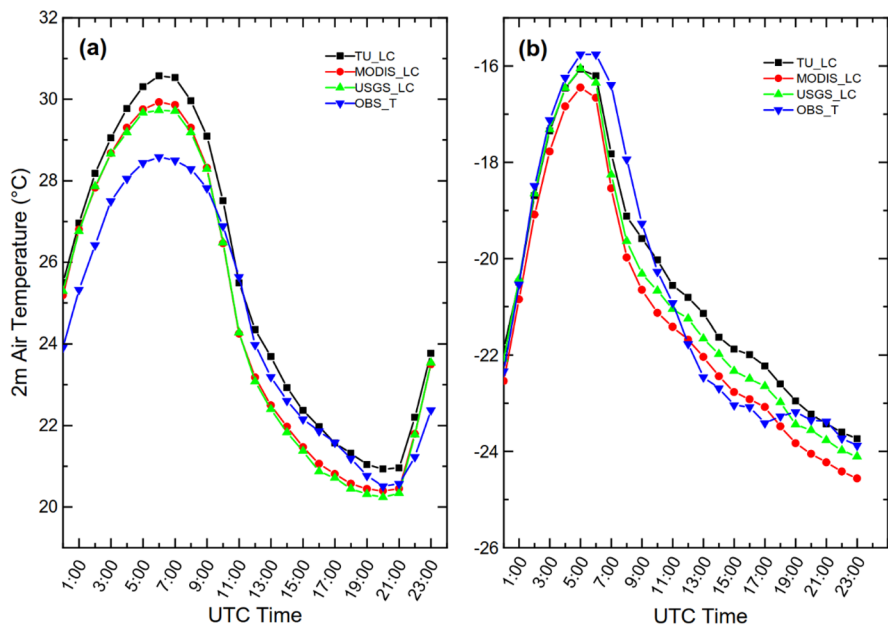
be deduced that the T_{2m} of the TU-based simulations have good performance when compared with MODIS and USGS-based simulations in the downtown Harbin and satellite towns stations. Similarly, the summer simulated T_{SK} was compared with the MODIS observation data (obtained on August 2, 2019, at 1:30 pm UTC), as shown in Supplementary Table S1. The results are categorized based on urban, suburban, and rural areas. The absolute MB of the urban T_{SK} for TU, MODIS, and USGS data were 1.18 °C, 1.03 °C, and 1.93 °C, respectively. Likewise, the RMSE of the urban T_{SK} for TU, MODIS, and USGS data were 1.18 °C, 1.03 °C, and 1.98 °C, respectively. In this case, the MODIS data was found to have the lowest MB and RMSE. Additionally, the MODIS reprojected result for the spatial variation for summer is shown in Supplementary Fig. S3.

During the winter simulations (Table 4), the TU land cover simulations had the lowest RMSEs of 5.67 °C, 5.48 °C, 4.54 °C, 5.88 °C, and 5.46 °C for Acheng, Bayan, Binxian, Harbin, and Hulan, respectively. The TU had most of the lowest absolute MBs of 3.55 °C (Acheng), 1.53 °C (Binxian), 3.38 °C (Harbin), and 2.11 °C (Hulan); while the USGS had 1.67 °C (Bayan). The strongest correlation value of 0.84 was observed at Binxian (for both TU and USGS) and Hulan (TU), while the lowest value of 0.77 was observed at both Acheng (USGS) and Harbin (TU). We further evaluated the winter T_{2m} using the Taylor diagram shown in Supplementary Fig. S2. The TU data performed better at Binxian and Acheng than MODIS and USGS data. For the winter simulated T_{SK} shown in Supplementary Table S1, the simulated T_{SK} was compared with the MODIS observation data (obtained on December 17, 2019, at 1:30 pm UTC). The TU data had the lowest absolute MB of 0.59 °C for the urban

area, followed by USGS and MODIS data accounting for 1.19 °C and 1.54 °C, respectively. Similarly, the TU data had the lowest RMSE of 0.65 °C with USGS and MODIS data accounting for 1.25 °C and 1.57 °C, respectively. Generally, from the results obtained, it can be deduced that the TU land cover simulation had performed relatively better than the MODIS and USGS data for T_{2m} and T_{SK} simulations. The outcome of the spatial coverage of the MODIS in winter is shown in Supplementary Fig. S4.

The diurnal variation evaluation results for the T_{2m} are shown in Fig. 2a, b. All comparisons were based on the UTC time scale (Beijing time will be UTC plus eight hours). In summer, all the simulations show good agreement when compared with the observation data during the daytime and nighttime, with TU_LC having the maximum temperature values at 6:00 UTC and 20:30 UTC. The USGS_LC has the lowest representation with the minimum temperature values both observed during the daytime and nighttime as well. The MODIS_LC is seen to be slightly above the USGS_LC at some points while at other points coincides. However, the three datasets showed an overestimation compared with observation data during the day, while MODIS_LC and USGS_LC showed an underestimation at night. In winter, all the simulations during the day showed underestimations with the MODIS_LC taking the minimum representation during the day at 6:00 UTC. The MODIS_LC showed the lowest temperature value while TU_LC was higher than USGS_LC. Moreover, at night, underestimations were observed for MODIS_LC and USGS_LC (17:30–23:00 UTC), while slight overestimations were observed for TU_LC. The TU_LC was also observed to have been underestimated between 12:00 and 17:30 UTC. The reason might be attributed to the

Fig. 2 Average diurnal variations between the measured and simulated T_{2m} , (a) summer and (b) winter (Note: Beijing time, LST = UTC + 8 h)



land surface properties response due to the predominant snow cover effect during winter. Similarly, the average hourly diurnal time series of the simulated T_{2m} of the different land cover datasets with observed data at downtown Harbin (Supplementary Figs. S5 and 6d) and satellite towns (Supplementary Figs. S5 and 6a–c, e) for both summer and winter, respectively, showed good agreement. Additional details can be found in the Supplementary information.

Impacts of land cover on surface energy fluxes

This section presents the results of the surface energy exchange due to the impact of land cover. As shown in Fig. 3, the monthly average sensible heat flux (SHF) with (a), (b), and (c) representing TU, MODIS, and USGS land cover datasets for summer, respectively, and (d), (e), and (f) representing the TU, MODIS, and USGS land cover datasets for the winter period, respectively. The black polygon line at the center of the map delineates downtown Harbin with the Songhua River cutting through the city. The satellite towns are represented with a solid dot in all the figures. The urban/built-up areas have the highest SHF due to the energy storage in the urban areas as a result of different surface materials used during construction. The TU built-up is seen to have the widest spatial coverage of energy storage. In the case of MODIS and

the USGS, the areas showing high radiation are only located in the central regions (Fig. 3a–c). The summer period of simulation shows that the absorbed energy from the urban surface is primarily attributed to the conserved sensible heat. The southeastern and the northeastern parts of the map are highly vegetated during the summer (Fig. 3a–c) in all the datasets. The lowest SHF was discovered on the water body which is seen to pass through the urban center. Next to the water body with the low sensible heat is the green areas which are predominantly covered by cropland/pasture land cover type, mostly covering areas like Binxian, Bayan, and part of Acheng which are predominantly cropland with some high-altitude areas. However, during the winter, because the sensible heat is very low, the urban/built-up is faintly seen. The green color, in this case, is not vegetation; instead, the surface is predominantly covered with snow, and most green plants hardly survived during this period; even if they do, they shade their leaves. The water body during this period freezes. The light blue color shows the mountainous area with the lowest SHF during the winter for TU, MODIS, and USGS land cover datasets. Moreover, the winter simulations for TU, MODIS, and USGS have a similar spatial pattern as the summer simulations. Nevertheless, the sensible heat flux is lower, which is due to the cooling effect of snowfall reflecting sunlight, resulting in a surface

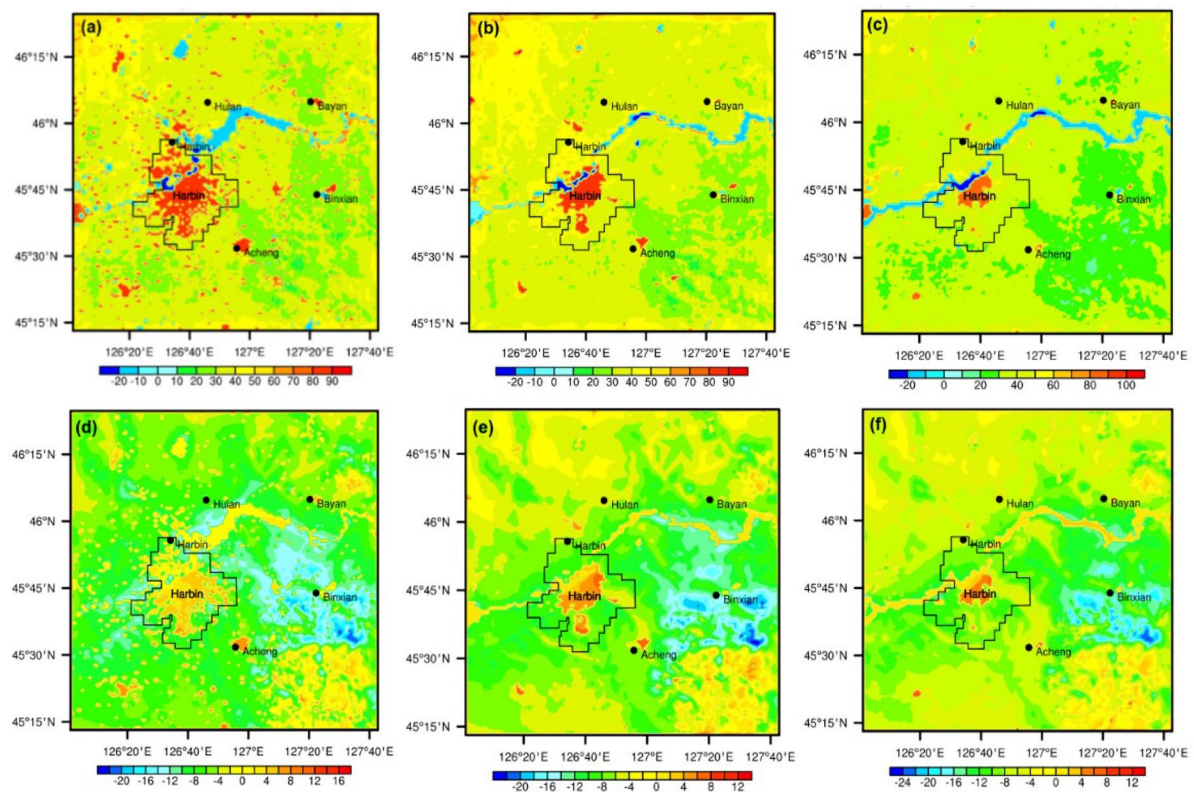


Fig. 3 Monthly average sensible heat flux (W/m^2): (a), (b), and (c) representing summer TU, MODIS, and USGS land cover data, respectively; and (d), (e), and (f) representing winter TU, MODIS, and USGS land cover data, respectively

temperature that is lower than the underlying surface temperature.

The monthly average latent heat flux (LHF) is shown in Fig. 4 with (a), (b), and (c) representing the TU, MODIS, and USGS results for summer, respectively, while (a), (b), and (c) represent the TU, MODIS, and USGS results for winter, respectively. In summer, the results showed that the LHF is higher in the surroundings than in the urban centers of both downtown Harbin and the satellite towns accounting for a maximum value of $130 \text{ W}/\text{m}^2$ (TU and MODIS) and $120 \text{ W}/\text{m}^2$ (USGS). The urban centers contributed less than $40 \text{ W}/\text{m}^2$ of the LHF. The lowest value was observed by the water body. The TU land cover has the widest spatial coverage compared with MODIS and USGS land cover datasets. During the winter period, the LHF is seen to be insignificant in the urban centers with maximum values of $10 \text{ W}/\text{m}^2$ (TU), $11 \text{ W}/\text{m}^2$ (MODIS), and $12 \text{ W}/\text{m}^2$ (USGS) around the mountainous region

of the domain. This insignificant effect is attributed to the large snow cover during this period. Generally, the SHF contributed more than the LHF to the earth's surface energy budget, hence enhancing UHI.

Urban heat island influenced by the land cover transformation

Spatial variations of land cover impact on the simulated T_{SK}

Figures 5 and 6 showed the seasonal spatial variations in the average simulated T_{SK} for summer and winter, respectively. During the summer period, Fig. 5a–c represents the average daytime (6:00 UTC or 14:00 LST) spatial variations while Fig. 5d–f shows the nighttime (14:00 UTC or 22:00 LST) spatial variations of the simulated T_{SK} for the TU, MODIS, and USGS land cover datasets, respectively. These three datasets accounted for the

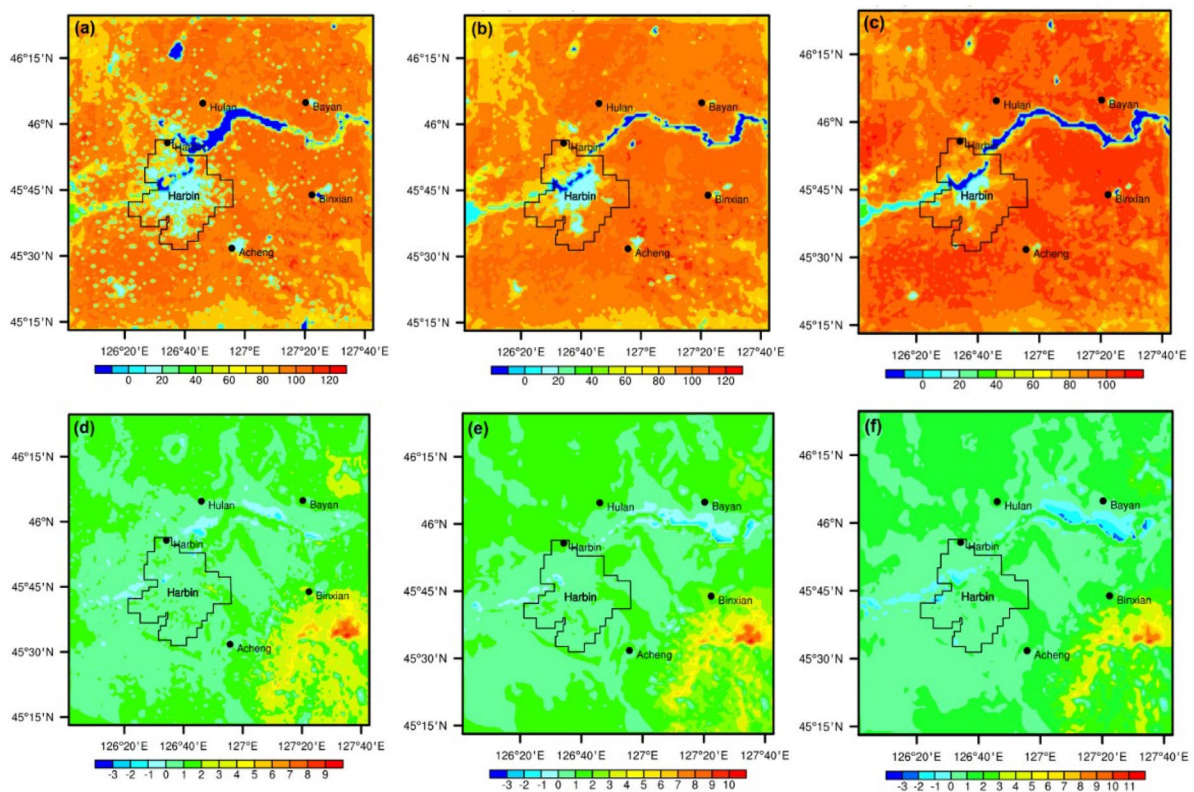


Fig. 4 Monthly average latent heat flux (W/m^2) for the period of simulation. (a), (b), and (c) represent summer TU, MODIS, and USGS land cover data, respectively; and (d), (e), and (f) represent winter TU, MODIS, and USGS land cover data, respectively

changes in the 2010s, 2000s, and 1990s, respectively. The TU land cover simulation showed a distinct spatial variation and the largest area impacted by temperature in both the urban core and the surrounding satellite towns compared with the MODIS and USGS land cover datasets, which is attributed to the rapid development in recent years due to the conversion of majorly cropland and grassland into urban/built-up land categories. The TU land cover showed the widest spread of the surface skin temperature compared with the MODIS and USGS land cover datasets. The intensity of the T_{SK} is concentrated within the urban centers of both downtown Harbin and the satellite towns across the three datasets with daytime having a wider spread than nighttime. This could be attributed to the radiation effect during the daytime. The urban/built-up land cover type has the maximum average T_{SK} of 23°C , and the water body has the minimum average value of 17°C . Additionally, the southeastern and northeastern

parts of the domain had low temperatures for both daytime and nighttime simulations because of the forested and mountainous areas within the region. In contrast, the northwestern and southwestern parts of the domain revealed a similar phenomenon for both daytime and nighttime T_{SK} for all three datasets, which accounted for a greater variation in temperature than the other half of the domain.

Similarly, during the winter period of the simulation, Fig. 6a–c showed the average daytime (6:00 UTC or 14:00 LST) spatial variations, and Fig. 6d–f represents the average nighttime (14:00 UTC or 22:00 LST) spatial variations of the T_{SK} for the TU, MODIS, and USGS land cover datasets, respectively. The MODIS and USGS land cover datasets had the lowest T_{SK} value of -25°C compared with the TU land cover dataset (-24°C) for both daytime and nighttime. The minimum average T_{SK} is observed on the northeastern part of the maps. The southeastern part of all the maps has the maximum daytime and

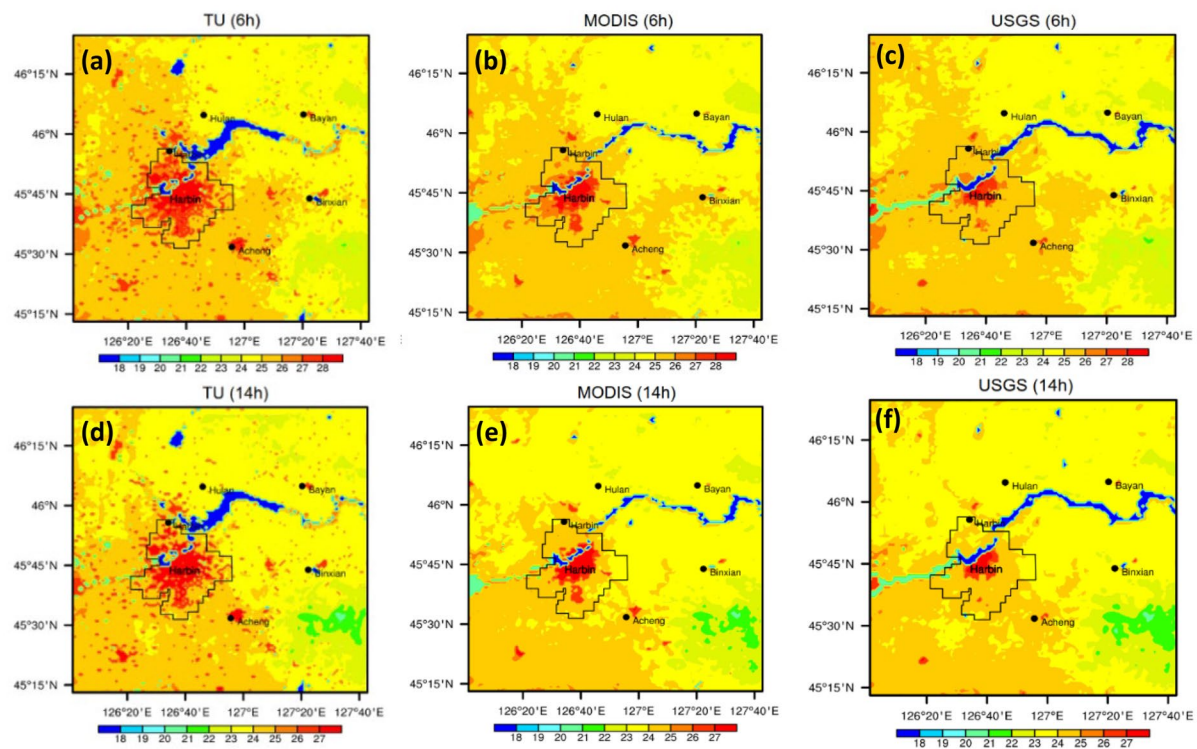


Fig. 5 Average summer surface skin temperatures ($^{\circ}\text{C}$): (a), (b), and (c) TU, MODIS, and USGS land cover data (6:00 UTC or 2:00 LST), respectively, and (d), (e), and (f) TU, MODIS, and USGS land cover data (14:00 UTC or 22:00 LST), respectively

nighttime average T_{SK} value of -15°C for the TU and the USGS land cover datasets and -16°C for the MODIS land cover data. It can be observed generally that the effect in winter is directly opposite to what is obtainable during the summer period. This could be a result of heavy snowfall which is predominant in this region.

Spatial variations of land cover impact on simulated T_{2m}

Figures 7 and 8 showed the seasonal spatial variations in the average simulated T_{2m} for summer and winter, respectively. In the summer season, Fig. 7a–c presents the daytime (6:00 UTC or 14:00 LST) and Fig. 7d–f nighttime (14:00 UTC or 22:00 LST) spatial variations of the simulated T_{2m} for the TU, MODIS, and USGS land cover datasets. The areas with high-temperature values of the TU land cover dataset for the daytime and nighttime (Fig. 7a, d) simulations are not only limited to the central regions of both the downtown Harbin and the satellite towns but can also

be seen spreading toward the surrounding areas (suburban/rural). The daytime and nighttime maximum average T_{2m} for the TU land cover data were found to be 26.5°C and 26°C , respectively, while MODIS and USGS land cover datasets accounted for an average T_{2m} value of 26°C in both daytime and nighttime. The minimum average T_{2m} value for the water body was found to be 20.5°C for both daytime and nighttime. We observed that the satellite towns (e.g., Acheng and Hulan) presented a significant spatial increase in air temperature for TU land cover data (in the 2010s) compared with USGS land cover data (in the 1990s); however, these changes may appear slight. The T_{2m} showed a similar pattern as the T_{SK} , whereas the USGS (Fig. 7c, f) and the MODIS land cover data (Fig. 7b, e) simulations presented high temperatures primarily in the urban center while TU land cover showed high temperatures spreading from the urban core to the surrounding regions. The USGS and MODIS land cover simulations also showed more homogeneous spatial patterns, while the TU land cover simulation showed more heterogeneous

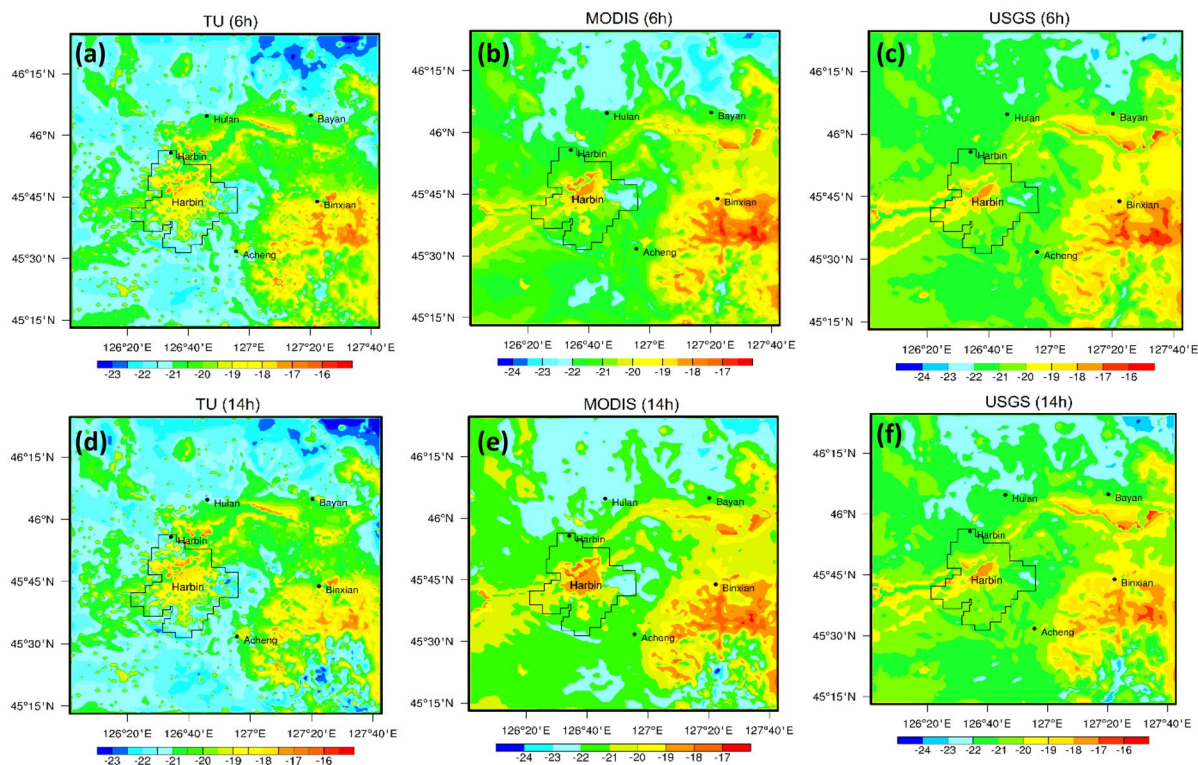


Fig. 6 Average winter surface skin temperatures ($^{\circ}\text{C}$): (a), (b), and (c) TU, MODIS, and USGS (6:00 UTC or 2:00 LST), respectively, and (d), (e), and (f) TU, MODIS, and USGS (14:00 UTC or 22:00 LST), respectively

patterns. Additionally, similar spatial patterns were observed in the southeastern part of all the maps and had lower air temperatures than the southwestern part. Likewise, the northeastern area of all the maps had a lower air temperature than the northwestern area of the maps. The northeastern/southeastern parts of all the maps are more vegetated than the northwestern/southwestern parts accounting for mostly cropland/pasture, forest, and mountainous. This is observed for daytime and nighttime across all the simulations corresponding to the TU, MODIS, and USGS land cover datasets.

During the winter period, Fig. 8a–c showed the spatially simulated average daytime T_{2m} and Fig. 8d–f showed the spatially simulated average nighttime T_{2m} variations corresponding to the TU, MODIS, and USGS land cover datasets. The mean lowest T_{2m} was observed during the nighttime. Compared with the TU land cover simulation, the USGS land cover simulation showed that the minimum average air temperature value of -21°C (colder) was

observed during the daytime toward the north and south of downtown Harbin (Fig. 8c). There is a significant spatial variation observed between the USGS and the TU land cover datasets, with an increase in the T_{2m} at the urban center than in its surroundings. Likewise, the surroundings were colder compared to the urban center at night, which could be a result of coal-burning and the heating mechanisms used to warm the urban center during the winter period. The southeastern to northeastern parts of the maps were observed to be dominated by vegetation, forest, and mountain land categories. This showed significant air temperature variations compared with their surroundings. During the winter period, the vegetation is grossly affected by the snow cover, hence having a different response to radiation compared to other land cover types. Generally, the nighttime T_{2m} and T_{SK} varied significantly compared to daytime T_{2m} and T_{SK} across the representative scenarios of the 2010s (TU) and 2000s (MODIS and 1990s USGS), while the differences in the 2010s were the most noticeable.

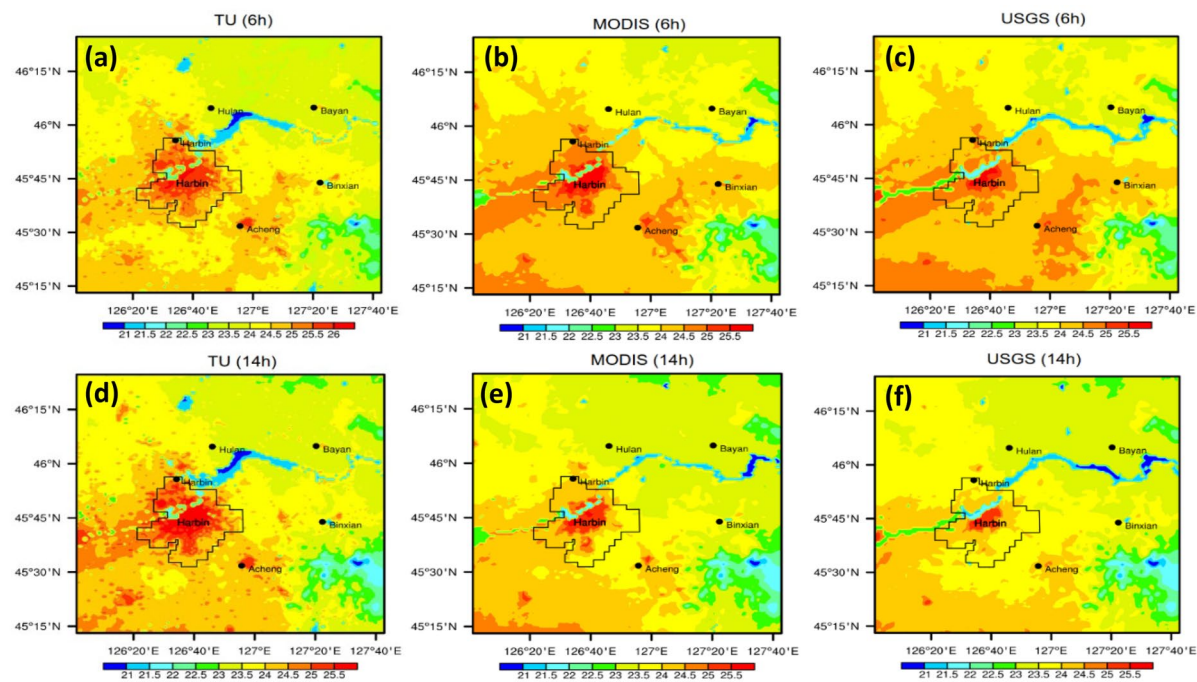


Fig. 7 Average summer 2-m air temperatures ($^{\circ}\text{C}$): (a), (b), and (c) TU, MODIS, and USGS (6:00 UTC or 2:00 LST), respectively, and (d), (e), and (f) TU, MODIS, and USGS (14:00 UTC or 22:00 LST), respectively

Long-term land cover transformation impact on UHI

Figure 9 showed the spatial daytime (6:00 UTC or 14:00 LST) and nighttime (14:00 UTC or 22:00 LST) simulated T_{2m} differences for both summer and winter represented in Fig. 9a–d, respectively. The simulated T_{2m} difference between the USGS-based simulation accounting for the 1990s (default dataset) and the TU-based simulation accounting for the 2010s (new dataset). These represented scenarios were chosen based on the datasets to account for the long-term changes in both T_{2m} and T_{SK} for daytime, nighttime, and seasonal variations. In summer, the intensity of the nighttime air temperature difference between the TU and USGS land cover datasets is higher and denser (in Fig. 9b) than that in the daytime (in Fig. 9a). These changes were also observed in the satellite towns (Acheng, Bayan, Binxian, and Hulan). The difference between the TU and the USGS land cover datasets depicts the spatial extent of the T_{2m} as a result of urban growth from the land cover variations. For both daytime and nighttime, significant differences were observed between downtown Harbin and the satellite towns, as well as its surroundings.

revealed the UHI phenomenon. Statistically, Table 5 further demonstrated that the nighttime T_{2m} UHI was higher than the daytime UHI. During the nighttime, Harbin, Acheng, Hulan, Binxian, and Bayan accounted for 1.25 $^{\circ}\text{C}$, 0.83 $^{\circ}\text{C}$, 0.78 $^{\circ}\text{C}$, 0.71 $^{\circ}\text{C}$, and 0.47 $^{\circ}\text{C}$, respectively, and during the daytime, Harbin and Binxian accounted for 0.57 $^{\circ}\text{C}$ each and Acheng, Bayan, and Hulan accounted for 0.34 $^{\circ}\text{C}$, 0.25 $^{\circ}\text{C}$, and 0.21 $^{\circ}\text{C}$, respectively. These statistical results were extracted based on the buffer designed at 5 km and 10 km. These delineated the area between urban centers and their surrounding rural counterparts. Similarly, during the winter period, Fig. 9c, d showed the T_{2m} difference between the TU-based simulation and the USGS simulation. The daytime and nighttime spatial variation were slightly noticeable and not as obvious as that for the summer period of T_{2m} (Fig. 9a, b). This result was associated with the peak snowfall during the winter period. These changes are seen from the urban area toward the northern part of the downtown and the southeastern part of the domain. However, the nighttime difference for T_{2m} is higher than the daytime, which is similar to the trend observed during summer. Table 5 further confirmed that the

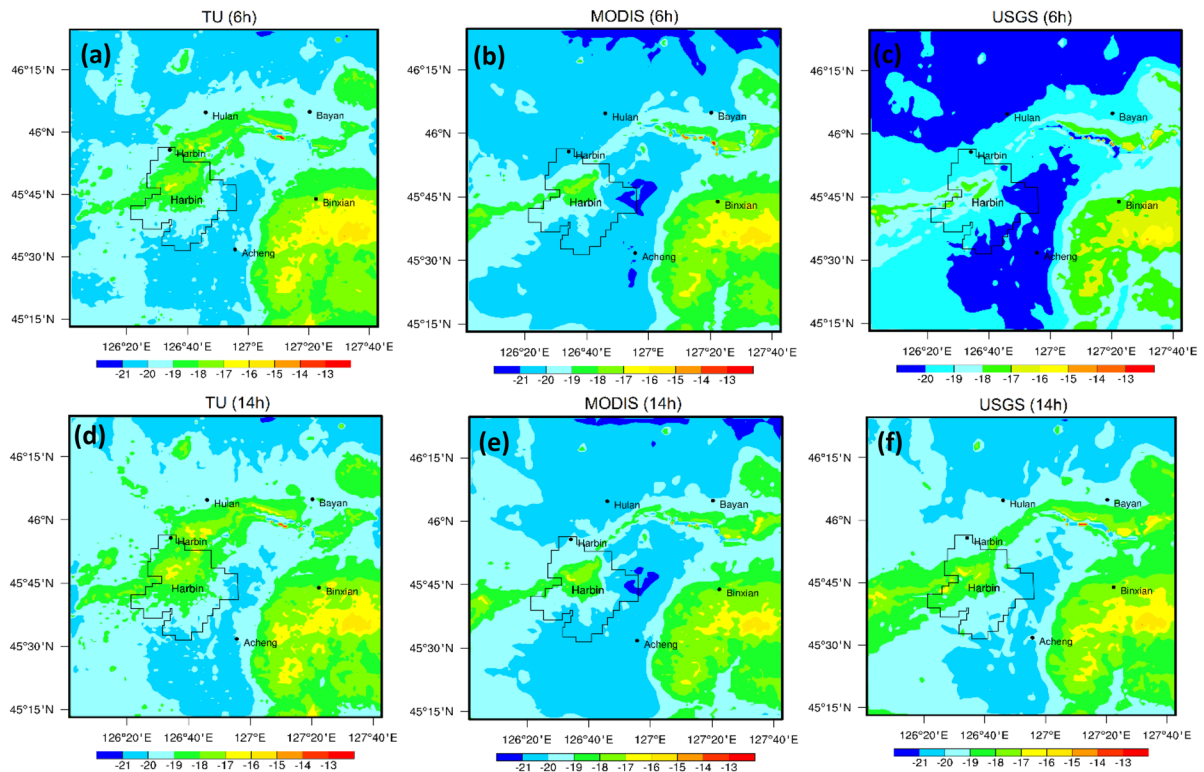


Fig. 8 Average winter 2-m air temperatures ($^{\circ}\text{C}$): (a), (b), and (c) TU, MODIS, and USGS (6:00 UTC or 2:00 LST), respectively, and (d), (e), and (f) TU, MODIS, and USGS (14:00 UTC or 22:00 LST), respectively

nighttime difference of $T_{2\text{m}}$ for Harbin ($0.20\ ^{\circ}\text{C}$), Hulan ($1.73\ ^{\circ}\text{C}$), Acheng ($0.28\ ^{\circ}\text{C}$), Bixian ($-0.19\ ^{\circ}\text{C}$), and Bayan ($-0.17\ ^{\circ}\text{C}$) were higher than the daytime $T_{2\text{m}}$ for Harbin ($0.15\ ^{\circ}\text{C}$), Hulan ($1.19\ ^{\circ}\text{C}$), Acheng ($0.26\ ^{\circ}\text{C}$), Bixian ($-0.36\ ^{\circ}\text{C}$), and Bayan ($-0.41\ ^{\circ}\text{C}$), respectively. Similar results can be seen for nighttime and daytime at 5 km and 10 km for the satellite towns and the downtown, respectively (see Table 5).—

Moreover, Fig. 10 showed the spatial differences in simulated T_{SK} for summer (a, b) daytime and the nighttime and winter (c, d) daytime and nighttime, respectively. During the summer period, we discovered spatially that there is a slight variation between the daytime and nighttime. The intensity during the nighttime is not too significant when compared with the summer effect. The spatial extent of the T_{SK} was observed to be more significant in downtown Harbin than in its surroundings; likewise, the core of the satellite towns and their surroundings. Furthermore, Table 5 also consolidated the fact that the nighttime difference in T_{SK} is higher

than in the daytime. For example, the summer difference in T_{SK} (nighttime > daytime) for urban centers of Harbin ($1.66\ ^{\circ}\text{C} > 1.25\ ^{\circ}\text{C}$), Hulan ($1.13\ ^{\circ}\text{C} > 0.66\ ^{\circ}\text{C}$), Acheng ($1.30\ ^{\circ}\text{C} > 0.89\ ^{\circ}\text{C}$), Bixian ($1.45\ ^{\circ}\text{C} > 1.68\ ^{\circ}\text{C}$), and Bayan ($0.79\ ^{\circ}\text{C} > 0.59\ ^{\circ}\text{C}$). Similarly, the difference in T_{SK} (nighttime > daytime) for the suburban/rural areas at 10 km for Harbin ($0.96\ ^{\circ}\text{C} > 0.59\ ^{\circ}\text{C}$) and at 5 km for Hulan ($0.22\ ^{\circ}\text{C} > -0.96\ ^{\circ}\text{C}$), Acheng ($0.49\ ^{\circ}\text{C} > 0.35\ ^{\circ}\text{C}$), Bixian ($0.20\ ^{\circ}\text{C} > 0.14\ ^{\circ}\text{C}$), and Bayan ($0.32\ ^{\circ}\text{C} > 0.21\ ^{\circ}\text{C}$). In winter, Fig. 10c, d showed the daytime and nighttime differences for simulated T_{SK} . During this season, a slight difference was observed between the daytime and nighttime along the southeastern part of the domain toward the northeastern part. This could be a result of the shortwave radiation effect during the daytime. The urban center seems not to have significant variation spatially. This could be attributed to the heavy snowfall in the winter period. Statistically, Table 5 confirmed the winter spatial variation result of the difference in T_{SK}

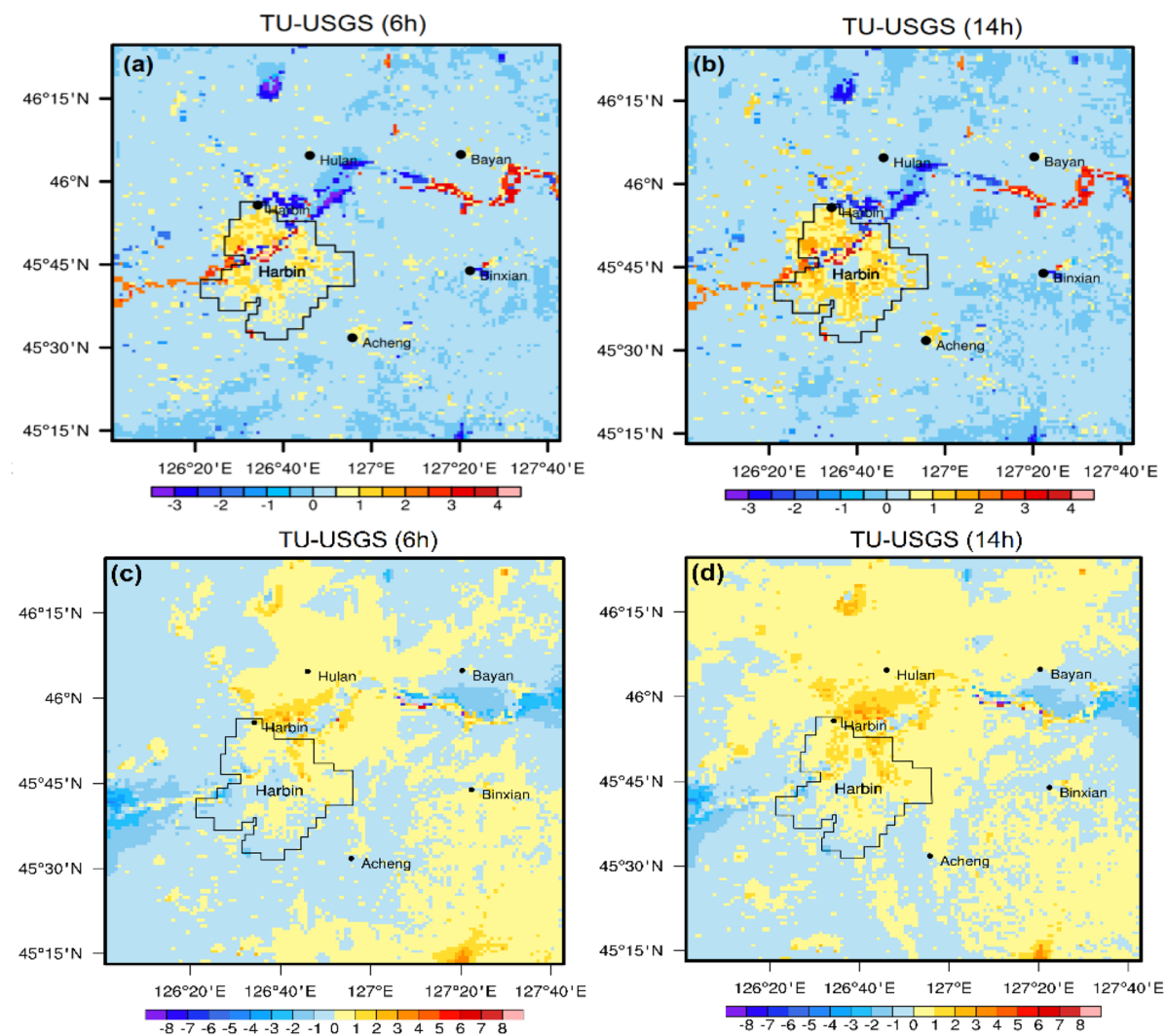


Fig. 9 Differences in 2-m air temperature ($^{\circ}\text{C}$) between TU and USGS (6:00 UTC or 2:00 LST and 14:00 UTC or 22:00 LST). Note: (a) and (b) represent summer, while (c) and (d) represent winter

for nighttime greater than daytime for Harbin ($0.10^{\circ}\text{C} > -0.09^{\circ}\text{C}$), Hulan ($2.75^{\circ}\text{C} > 1.98^{\circ}\text{C}$), Acheng ($0.64^{\circ}\text{C} > 0.56^{\circ}\text{C}$), Binxian ($-1.05^{\circ}\text{C} > -1.20^{\circ}\text{C}$), and Bayan ($0.83^{\circ}\text{C} > 0.11^{\circ}\text{C}$). Likewise, a similar pattern was observed for the surroundings of the urban centers of the downtown and the satellite towns. The heavy snow cover during this season has a great effect on the results with Hulan satellite town having the highest difference for $T_{2\text{m}}$ and T_{SK} in both daytime and nighttime.

Discussion

UHI in Harbin has increased significantly as a result of changes in land cover over the years. The UHI was investigated using a new TU land cover dataset compared with the WRF default datasets (USGS and MODIS). The simulated results were evaluated using the observation data from meteorological stations and MODIS (LST). In this study, we observed that the $T_{2\text{m}}$ of Hulan (a satellite town station) had

Table 5 Average simulated T_{SK} ($^{\circ}\text{C}$) and T_{2m} ($^{\circ}\text{C}$) values within domain 4 for the TU and USGS land cover simulations

Season	Location	TU (2010s)		USGS (1990s)		Difference (TU-USGS)	
		Daytime		Nighttime		Daytime Diff	
		T_{2m}	T_{SK}	T_{2m}	T_{SK}	T_{2m}	T_{SK}
Summer	DT_1_Harbin	25.87	28.02	23.14	22.71	25.30	26.77
	DT_2_Harbin_Buffer_10km	25.59	27.33	22.37	21.55	25.29	26.74
	ST_1_Hulan	25.77	28.15	22.18	21.77	25.56	27.49
	ST_2_Hulan_Buffer_5km	25.08	26.22	21.55	20.40	25.46	27.18
	ST_1_Acheng	25.85	28.09	22.42	22.03	25.51	27.20
	ST_2_Acheng_Buffer_5km	25.57	27.21	21.92	20.95	25.38	26.86
	ST_1_Binxian	25.57	27.93	21.98	21.81	25.00	26.25
	ST_2_Binxian_Buffer_5km	25.02	26.42	21.42	20.21	24.93	26.29
	ST_1_Bayan	25.34	27.59	21.21	20.87	25.08	27.00
	ST_2_Bayan_Buffer_5km	25.11	26.68	20.84	19.80	24.94	26.47
Winter	DT_1_Harbin	-17.39	-15.84	-18.73	-18.21	-17.54	-15.75
	DT_2_Harbin_Buffer_10km	-18.01	-17.01	-19.49	-19.63	-18.24	-17.47
	ST_1_Hulan	-17.83	-17.87	-19.59	-20.88	-19.02	-19.85
	ST_2_Hulan_Buffer_5km	-16.88	-14.74	-18.41	-17.45	-19.07	-20.04
	ST_1_Acheng	-19.14	-19.26	-21.07	-22.12	-19.40	-19.82
	ST_2_Acheng_Buffer_5km	-19.15	-19.67	-20.93	-22.56	-19.24	-19.80
	ST_1_Binxian	-16.89	-17.21	-18.26	-19.61	-16.53	-16.01
	ST_2_Binxian_Buffer_5km	-17.33	-17.96	-18.82	-20.68	-17.32	-18.04
	ST_1_Bayan	-19.13	-19.61	-20.78	-22.44	-18.71	-19.72
	ST_2_Bayan_Buffer_5km	-19.20	-20.19	-20.80	-23.23	-18.73	-19.92

DT 1 and DT 2 represent the downtown center and surrounding at a 10 km buffer. ST 1 and ST 2 represent satellite towns center and their surroundings at 5 km, respectively. T_{2m} and T_{SK} are temperatures at 2-m and surface skin, respectively

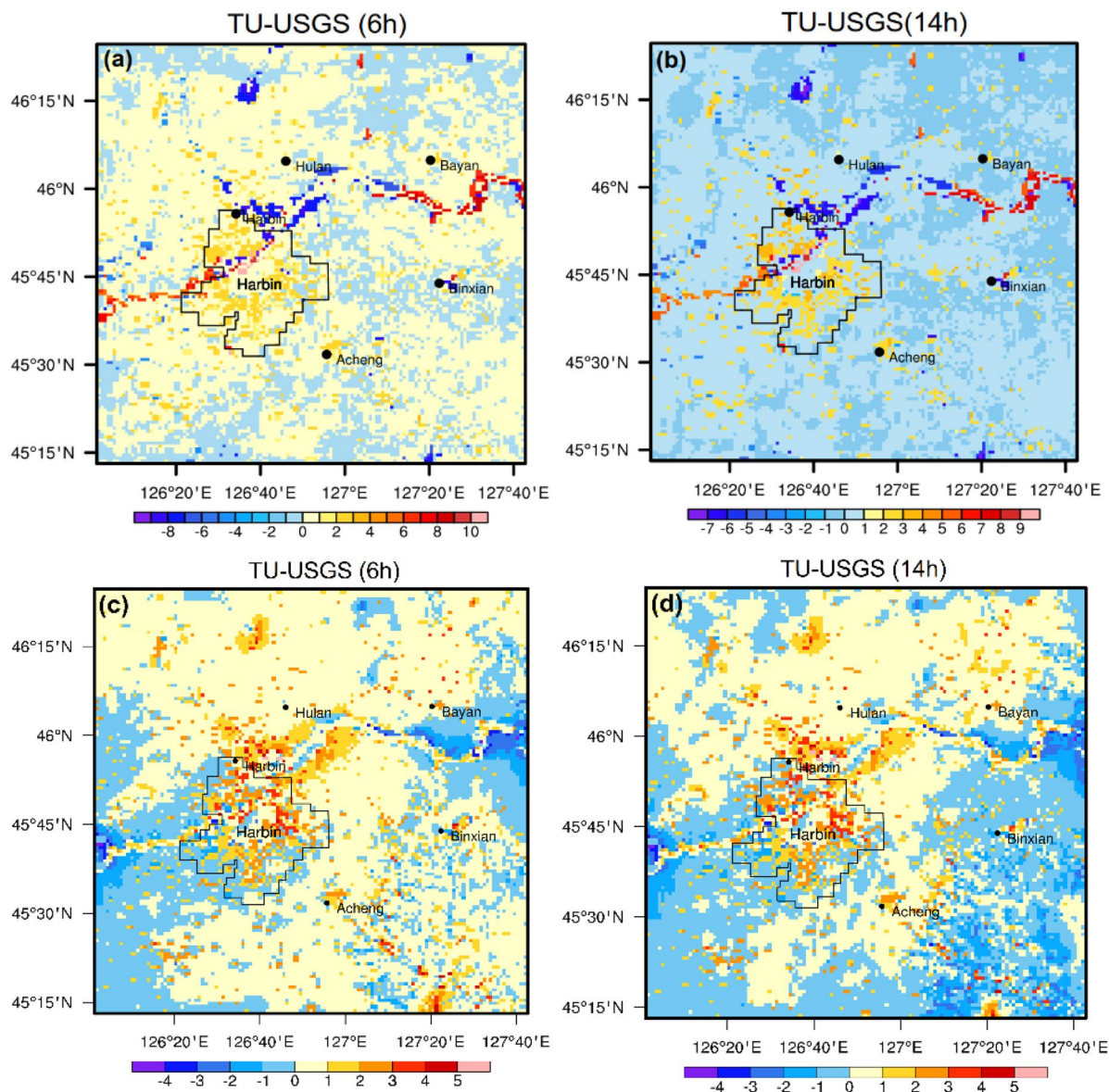


Fig. 10 Differences in surface skin temperature ($^{\circ}\text{C}$) between TU and USGS (6:00 UTC or 2:00 LST and 14:00 UTC or 22:00 LST). Note: (a) and (b) represent summer, while (c) and (d) represent winter

the best performance in both summer and winter, followed by Bayan (summer) and Binxian (winter). These results agree with the Taylor diagram in Supplementary Figs. S1 and S2, where the closest point to the reference (REF) point is termed to have good performance. The summer and winter results for T_{2m} and T_{SK} revealed that the TU land cover simulation had a good performance and the strongest correlation over MODIS and USGS land cover datasets. A

previous study by Li et al. (2018a, b) also revealed the good performance of a new dataset (CORINE) over the default USGS dataset. Similarly, the evaluation between simulated T_{SK} and the MODIS observation data (LST) revealed that the TU land cover data performed relatively better than MODIS and USGS in both summer and winter. A study by Li et al. (2020) reported the usefulness of a new GLC2015 land-use dataset in improving the performance of the

WRF model in the summer months. From the diurnal evaluation of T_{2m} , the findings showed that TU land cover is suitable for the simulation of UHIs due to its heterogeneity, which is in agreement with the study of Huidong (2018). This study also revealed that the T_{2m} was very low for all three datasets at night and in the early hours of the day because of snowfall during winter. For the two seasons, the daytime simulations had a similar pattern while the nighttime simulations showed distinct variations. The study by Huang and Gao (2018) attributed the changes in weather processes to the reanalysis data, which played a significant role in the model simulation.

The sensible and latent heat were considered in this study to determine the heat transfer between airflow and surfaces. The production of UHI is aided by heat storage fluxes inside metropolitan areas (Mirzaei & Haghishat, 2010). The study of UHI is associated with the impact of land cover, which determines the earth's surface energy budget. Land surface property variations lead to UHIs which are based on differences in the energy budgets between urban and suburban/rural areas (Oke, 1982, 1988). The TU, MODIS, and USGS land cover datasets were utilized in this study to investigate the mechanisms underlying the different performances of the three land cover simulations and the circulation of the average surface energy balance elements. The spatial extent of the TU-based land cover simulation exceeds that of the MODIS and USGS-based land cover simulations, with the TU-based simulation accounting for the greatest sensible heat flux not only in the city center but also in the surrounding environments extending to the satellite towns. Moreover, the largest allotment to the stored sensible heat flux of the TU-based land cover simulations makes the urban core warmer than its surrounding areas. Likewise, the urban centers of the MODIS and USGS-based simulations were warmer than their surroundings. However, during the nighttime, when solar radiation vanishes, the stored energy at the surface is subsequently removed as a source of energy to counteract the cooling effect on the surface. During the daytime, the urban surface discharges energy more than the natural surface as a result of increased energy storage in urban areas, hence conserving the UHI phenomena at night because this increased heating during the day is offset by more prolonged sensible heat and longwave radiative fluxes at the urban surface at night. This finding is consistent with the

study by Kim et al. (2021) which also revealed an increase in the energy storage in urban areas during the day and emits it at night. Moreover, the winter simulations for TU, MODIS, and USGS land cover datasets have a similar spatial pattern as the summer simulations. Nevertheless, the sensible heat flux is lower, which is due to the cooling effect of snowfall reflecting sunlight, resulting in a surface temperature that is lower than the underlying surface temperature. From Eq. (4), considering the same quantity of radiation, the amount of heat stored on the surface will decrease provided that more shortwave radiation is reflected in the sky; hence, sensible heat is formed through turbulence after the atmosphere is heated by longwave radiation (Mirzaei & Haghishat, 2010; Kirthiga & Patel, 2018; Li et al., 2020). The latent heat flux for summer takes a similar pattern to the sensible heat flux across the three datasets, with TU-based simulation having more of an effect in the urban center than in the surrounding areas; this agrees with the study of Jain et al. (2021). However, the LHF has an insignificant effect due to the large extent of coverage by snowfall in winter across the three datasets. Therefore, sensible and latent heat contributes significantly to the formation of UHI.

The spatial variations of the influence of land cover on the simulated T_{SK} revealed that the TU-based simulation had a distinct spatial variation and the largest area impacted by the T_{SK} in both the urban core and the surrounding satellite towns compared with the MODIS and USGS land cover datasets. The reason could be attributed to the rapid development in recent years due to the conversion of majorly cropland and grassland into urban/built-up land categories. The study by Xiaolin (2017) also highlighted this as a possible reason. It is worth noting that the default USGS-based land cover dataset incorporated in the WRF model is unable to accurately depict the current urbanization process and hence underestimates the UHI spatial extent. Although the MODIS land cover dataset was incorporated into the model in the early 2000s, it has not been updated compared with the rapid development in the region. However, the USGS and MODIS-based land cover simulations showed that the UHI effect was primarily concentrated in the central part of Harbin with a similar pattern also seen in the study of Huidong (2018), where the urban core in Berlin was observed to have more effect of UHI than its surroundings. Moreover,

noticeable changes were observed in the satellite towns from the TU land cover compared with the MODIS and USGS land cover datasets. These land cover transformations within the satellite towns have impacted the UHIs mainly in the satellite town cores rather than the surrounding rural areas because of the conversion of major cropland/pasture and grassland to the urban/built-up land category. It was also observed that the intensity of the T_{SK} is greater during the day than at night; this is a result of the influence of shortwave radiation. This agrees with the study by Mirzaei and Haghigat (2010). During the winter period, the effect is directly opposite to what is obtainable during the summer period. The differences observed between the three land cover datasets are attributed to the compact nature of the urban environment and the effect of rapid urbanization and the anthropogenic heat (AH) effect updated during the model simulation. Moreover, the influence of the AH is greater in winter than in summer, which agrees with the study of Ichinose et al. (1999). However, a contrasting effect is observed in winter, showing that the southeastern part of the domain, downtown Harbin, and satellite towns have slightly higher surface skin temperatures than the northeastern/southern parts of the domain compared to the summer period. This could be attributed to the coal-burning activities during this season and the mountainous influence in the southeastern part. It was also observed that the mean T_{SK} values for both summer and winter were higher during the day than at night, which was attributed to the strong dependence on the land cover datasets. A previous study by Li et al. (2020) also confirmed this strong dependence on the land cover by incorporating a new multi-satellite remote-sensing GLC2015 land-use data with 300 m spatial resolution in the WRF model. Therefore, due to the dependence of T_{SK} on land cover, it becomes necessary to investigate its spatial extent because it contributes significantly to the T_{2m} .

The spatial variation of the impact of land cover on simulated T_{2m} showed that the USGS and MODIS-based simulations had more homogeneous spatial patterns, while the TU-based simulation showed more heterogeneous patterns. The spatial distributions of T_{2m} are finer than that of T_{SK} across the three land cover datasets. However, the T_{SK} depends more on the land cover dataset, unlike T_{2m} , which can be impacted by air advection (Azevedo et al., 2016; Huidong, 2018).

During the daytime, the simulated T_{2m} based on the TU, MODIS, and USGS land cover is consistently less than the simulated T_{SK} . Additionally, lower temperature values were observed in the southeastern parts of the maps than in the southwestern part for three land cover datasets. During the winter period, the lowest average T_{2m} was observed during the nighttime. The USGS land cover simulation revealed that a minimum of T_{2m} occurred in the urban center during the day. Likewise, the surroundings appeared to be colder compared to the urban center at night, which could be a result of coal-burning and the heating mechanisms used to warm the urban center during the winter period. It is worth noting that Harbin is the coldest megacity in China and has large areas covered with snowfall, resulting in a lower temperature than that of the underlying surface influenced by the surface albedo (Huang et al., 2018). Additionally, winter temperatures are greatly influenced by anthropogenic heat, which is consistent with studies by Shahmohamadi et al. (2011) and Ichinose et al. (1999). Therefore, this study observed a trend in which the urban center of downtown Harbin presented a significant variation in temperature when compared with its suburban and rural counterparts, hence revealing the UHI phenomenon. Alternatively, rural/suburban regions are colder than the urban core. Satellite towns are gradually experiencing the effect of UHI when compared with their surroundings at a 5 km buffer. Although the spatial changes may appear small but are statistically significant (see Table 5). Nighttime temperatures varied significantly compared to daytime temperatures across the representative scenarios of the 2010s (TU) and 2000s (MODIS), and 1990s (USGS), while the differences in the 2010s were the most noticeable. A previous study by Li et al. (2019) confirmed that UHI was pronounced at nighttime in Berlin. It also revealed that an increase in the impervious surface (ISA_{WRF}) linearly increased the simulated nighttime T_{2m} . Therefore, to understand the effect of UHI as it affects the thermal comfort of the population, it becomes significant to look at the simulated T_{SK} alongside the T_{2m} because these formed the basis for the investigation of UHI.

The spatial variation results from the long-term impact of land cover on UHI revealed that the nighttime UHI of T_{2m} and T_{SK} between the TU_LC (in 2017) and the USGS_LC (in 1993) was higher than the daytime UHI of T_{2m} and T_{SK} for summer and winter, respectively. Harbin was discovered to have the highest difference in T_{2m} and T_{SK} for nighttime and

daytime than all the satellite towns in the summer period. We discovered from the results in winter that Hulan had the highest difference in T_{2m} and T_{SK} for both nighttime and daytime. The possible reason is that Hulan is majorly bounded by the Songhua River, which is completely frozen and makes it colder than downtown Harbin and the other satellite towns. The intensity during the nighttime is not too significant when compared with the summer effect. The reason is that the shortwave radiation absorbed at the surface during the daytime is discharged during the nighttime, hence resulting in the small differences observed (Fig. 10a, b). Thus, nighttime showed no shortwave radiation effect but the influence of longwave radiation effect. Mirzaei and Haghhighat (2010) explained further that, when the sky is mainly clear and quiet, solar radiation has a substantial role in diurnal heat islands. Urban surfaces absorb some of the sun's rays and reflect some of them. Direct and diffuse portions of incident solar energy are also present on surfaces. The studies by Zhou and Chen (2018) and Kim et al. (2021) also highlighted the dominant role played by anthropogenic heat in the nighttime surface energy balance. Additionally, the temperature variations could be attributed to the discharge of the energy stored in the urban surfaces, which agrees with previous studies (Oke, 1995; Gedzelman et al., 2003 Huidong, 2018). Moreover, this study further revealed that the daytime for the USGS land cover was underestimated compared with TU and MODIS land cover data. The studies of Cheng et al. (2013) and Bhati and Mohan (2016) also showed that daytime temperatures were underestimated when using the USGS dataset in western Taiwan and Delhi, as a result, underestimated urban areas.

Interestingly, the satellite towns that were barely noticed in the USGS-based land cover simulation are noticeable in the TU-based land cover simulation, hence resulting in a significant difference between the two land cover datasets (TU and USGS). We discovered from our results in Table 5 that the summer nighttime difference of T_{2m} in the core of the satellite towns is significant in Acheng, Hulan, and Binxian. Hence, the Acheng and Hulan UHIs are higher than those of the other satellite towns during the summer season. Comparatively, the daytime difference within the center of the satellite towns was more pronounced in Binxian and Acheng. Additionally, the Harbin daytime and nighttime UHIs for T_{2m} and T_{SK} were higher

than those of the satellite towns. This finding is attributed to the greater number of impervious surfaces associated with recent development and other human activities within the city and at the fringes. Moreover, the T_{2m} and T_{SK} within the urban centers for downtown Harbin and the satellite towns were higher than their surroundings for both daytime and nighttime in the summer period. Li et al. (2019) updated the urban canopy parameters using the impervious and vegetation component in the model, and their results confirmed an increase in the impervious surface (ISA_{WRF}) linearly increased the simulated nighttime T_{2m} . Our results from the winter season revealed that significant differences in daytime T_{2m} and T_{SK} occurred in the urban core of Hulan and Harbin compared with the surrounding regions. These significant differences could be attributed to the anthropogenic heat effect, which was updated during the simulation (Ichinose et al., 1999), and the coal-burning effect, which greatly influences the temperature within urban centers. Additionally, the frozen river in Hulan could account for the large differences observed in the two extreme years, 1993 (USGS) and 2017 (TU). However, a typical UHI pattern corresponding to daytime and nighttime was noticed within the satellite town centers of Acheng and Bayan compared to their surroundings, and a similar pattern was observed at the 5 km buffer for T_{2m} and T_{SK} in both cases. This pattern depicts a phenomenon in which the nighttime temperature is colder and the daytime temperature is warmer, which is consistent with the study conducted by Palou and Mahalov (2019) for T_{SK} and T_{2m} in both summer and winter periods. Additionally, in winter, the inherent surface is predominantly covered by snow, accounting for the slight variation noticed in the surface temperatures and its effect on UHIs. The significance of this is that it provides UHI information for investigating its interactions with air pollution and how it affects the climatic comfort of the city.

In general, the UHIs of downtown Harbin and the satellite towns depict a similar phenomenon commonly noticed in summer. Hence, the winter season revealed an interesting phenomenon in which the surroundings are significantly colder than the urban centers, thus indicating a typical cold island that is also impacted by the land cover transformation of the representative scenarios between the 1990s (USGS) and 2010s (TU). Moreover, it has been observed from this study and other studies that more heat is distributed

to the atmosphere from urban surfaces than the natural surface, which results in a warmer atmosphere in urban areas compared with their suburban/rural counterparts (Oke, 1982). The emission of atmospheric longwave radiation can potentially be increased by UHI-induced warming of the urban atmosphere.

Conclusion

In this study, we investigated the impact of land cover changes on the simulation of urban heat islands in Harbin city of China using the coupled WRF/SLUCM model. This model was effective in this study because of its high-resolution capacity and its superiority over in situ and remote sensing approaches in the study of UHIs. The new TU land cover data was compared with the two default datasets (USGS and MODIS). The simulated results were evaluated using the observed data in order to provide a basis for the reliability of the results. The results of this study showed that the new TU land cover dataset had a better representation and a good performance than the two default datasets in the WRF model. The TU-based land cover simulation performed better than the USGS and MODIS-based land cover simulations for both T_{SK} and T_{2m} in both summer and winter. We observed that the USGS-based land cover simulation underestimated the temperature, particularly in satellite towns and suburban areas. The TU-based land cover simulation reflected a more realistic spatial distribution of UHI than the default datasets within the domain and depicted properly the urbanization process in downtown Harbin and the surrounding satellite towns.

The study discovered that T_{SK} and T_{2m} are higher within the urban centers than in their surroundings for the three land cover datasets. Moreover, significant growth was observed around the satellite towns resulting in the rise of T_{SK} and T_{2m} . Due to rapid development in the surrounding regions of Harbin city and the satellite towns, more natural surfaces (that is, croplands, pasture lands, irrigated lands, etc.) have been transformed into impervious surfaces, thus leading to urban–rural temperature differences. Noticeable seasonal changes were observed from the TU, MODIS, and USGS-based simulations, which accounted for the significant variations in the T_{SK} and T_{2m} in the downtown Harbin and satellite towns.

The summer and winter long-term changes clearly showed that the T_{2m} and T_{SK} extracted from TU land cover data were generally higher than those extracted from USGS data. During summer, the temperatures within the urban core for downtown Harbin and the satellite towns were higher than those in the surroundings for both daytime and nighttime. Similarly, during winter, the temperature in the urban centers was higher than that in the surroundings of the downtown area and some satellite towns, indicating the effect of a cold/heat island phenomenon. This finding further indicates that the coal-burning activities within the urban centers provide a buffering effect against the cold within urban centers compared with the surroundings; thus, urban centers become more habitable for residents during this season. Additionally, the improved anthropogenic heat in the model enhanced the sensible and latent heat fluxes within residential areas. The SHF was closely associated with the T_{SK} and contributed significantly to land surface modifications, hence leading to a rise in T_{SK} compared to the T_{2m} . This further explained why the T_{2m} was influenced by thermal convection from surface heat exchange and longwave radiation.

It is worthy to note that our conclusions were drawn from land cover outcomes. These outcomes will be significant for understanding urban climate studies and providing the necessary insight into the study of bioclimatic comfort, which will be looked at in our future works. We recommend an up-to-date TU land cover dataset for WRF simulations for the northeast region of China. The same studies can be replicated in other parts of the world using a high-resolution dataset suitable for varieties of purposes. Moreover, the coupled WRF-SLUCM is an effective approach in the study of UHI and could be used in other studies related to urban climate for better performance. The findings here highlighted the need for environmental scientists and lawmakers to develop and implement mitigation strategies that will improve the bioclimatic comfort of Harbin from the effect of UHI.

Acknowledgements We sincerely acknowledged the contribution of Tsinghua University in developing the land cover dataset. We thank the Global Data Assimilation System (GDAS) for the provision of FNL forcing data and the MODIS open access data. Also, our gratitude goes to China Meteorological Data Service Center and Heilongjiang Provincial Environmental Monitoring Center for the observational data and the Mendeley Data Repository for the provision of reference

materials. We acknowledged the support of the Open Project of the State Key Laboratory of Urban Water Resource and Environment, Harbin Institute of Technology (No. HC202143), and the Heilongjiang Provincial Key Laboratory of Polar Environment and Ecosystem (HPKL-PEE) (No. 2021011).

Author contribution **Stephen Dauda Yabo:** conceptualization, data curation, methodology, formal analysis, writing – original draft preparation, writing – reviewing and editing. **Donglei Fu:** resources, methodology, software, writing – reviewing and editing. **Bo Li:** resources, software. **Xiaofei Shi:** resources, visualization, and validation. **Samit Thapa:** investigation, writing – reviewing and editing. **Xie Shengjin:** visualization and investigation. **LuLu:** resources and visualization. **Hong Qi:** resources, methodology, conceptualization, reviewing and editing, supervision, project administration, and funding acquisition. **Wei Zhang:** formal analysis, methodology, resources, validation.

Funding This work was supported by the Open Project of State Key Laboratory of Urban Water Resource and Environment, Harbin Institute of Technology (No. HC202143), and the Heilongjiang Provincial Key Laboratory of Polar Environment and Ecosystem (HPKL-PEE) (No. 2021011).

Data availability The datasets generated during the current study are available from the corresponding author on reasonable request.

Declarations

Conflict of interest The authors declare no competing interests.

References

- Adiguzel, F., Bozdogan Sert, E., Dinc, Y., Cetin, M., Gungor, S., Yuka, P., Sertkaya Dogan, O., Kaya, E., Karakaya, K., & Vural, E. (2022). Determining the relationships between climatic elements and thermal comfort and tourism activities using the tourism climate index for urban planning: A case study of Izmir Province: Tourism climate index for urban planning. *Theoretical and Applied Climatology*, 147(3–4), 1105–1120. <https://doi.org/10.1007/s00704-021-03874-9>
- Adiguzel, F., Cetin, M., Kaya, E., Simsek, M., Gungor, S., & Bozdogan Sert, E. (2020). Defining suitable areas for bioclimatic comfort for landscape planning and landscape management in Hatay, Turkey. *Theoretical and Applied Climatology*, 139(3–4), 1493–1503. <https://doi.org/10.1007/s00704-019-03065-7>
- Arghavani, S., Malakooti, H., & Bidokhti, A. A. A. A. (2020). Numerical assessment of the urban green space scenarios on urban heat island and thermal comfort level in Tehran Metropolis. *Journal of Cleaner Production*, 261, 121183. <https://doi.org/10.1016/j.jclepro.2020.121183>
- Azevedo, J. A., Chapman, L., & Muller, C. L. (2016). Quantifying the daytime and night-time urban heat Island in Birmingham, UK: A comparison of satellite derived land surface temperature and high resolution air temperature observations. *Remote Sensing*, 8(2). <https://doi.org/10.3390/rs8020153>
- Bhati, S., & Mohan, M. (2016). WRF model evaluation for the urban heat island assessment under varying land use/land cover and reference site conditions. *Theoretical and Applied Climatology*, 126(1–2), 385–400. <https://doi.org/10.1007/s00704-015-1589-5>
- Bozdogan Sert, E., Kaya, E., Adiguzel, F., Cetin, M., Gungor, S., Zeren Cetin, I., & Dinc, Y. (2021). Effect of the surface temperature of surface materials on thermal comfort: A case study of Iskenderun (Hatay, Turkey). *Theoretical and Applied Climatology*, 144(1–2), 103–113. <https://doi.org/10.1007/s00704-021-03524-0>
- Brovkin, V., Boysen, L., Arora, V. K., Boisier, J. P., Cadule, P., Chini, L., Claussen, M., Friedlingstein, P., Gayler, V., Van Den Hurk B. J., Hurt, G. C., Jones, J. D., Kato, E., De Noblet-Ducoudre, N., Pacifico, F., Ponratz, J., & Weiss, M. (2013). Effect of anthropogenic land-use and land-cover changes on climate and land carbon storage in CMIP5 projections for the twenty-first century. *Journal of Climate*, 26(18), 6859–6881. <https://doi.org/10.1175/JCLI-D-12-00623.1>
- Cao, F., Zhang, S. C., Kawamura, K., & Zhang, Y. L. (2016). Inorganic markers, carbonaceous components and stable carbon isotope from biomass burning aerosols in Northeast China. *Science of the Total Environment*, 572, 1244–1251. <https://doi.org/10.1016/j.scitotenv.2015.09.099>
- Cetin, M. (2015). Determining the bioclimatic comfort in Kas-tamonusu City. *Environmental Monitoring and Assessment*, 187(10). <https://doi.org/10.1007/s10661-015-4861-3>
- Cetin, M. (2016). *Türk Tarım - Gıda Bilim Ve Teknoloji Dergisi Peyzaj Planlamada Biyoklimatik Konfor Alanlarıın Belirlenmesi : Cide Kıyı Şeridi Örneği*, 4(9), 800–804.
- Cetin, M. (2019). The effect of urban planning on urban formations determining bioclimatic comfort area's effect using satellite imagines on air quality: A case study of Bursa city. *Air Quality, Atmosphere and Health*, 12(10), 1237–1249. <https://doi.org/10.1007/s11869-019-00742-4>
- Cetin, M. (2020a). Climate comfort depending on different altitudes and land use in the urban areas in Kahramanmaraş City. *Air Quality, Atmosphere and Health*, 13(8) 991–999. <https://doi.org/10.1007/s11869-020-00858-y>
- Cetin, M. (2020b). *Turkish Journal of Agriculture - Food Science and Technology The changing of important factors in the landscape planning occur due to global climate change in temperature, rain and climate types : A case study of Mersin City Peyzaj Planlama Aşamasında Ön. 8(12)*, 2695–2701.
- Cetin, M., Adiguzel, F., Gungor, S., Kaya, E., & Sancar, M. C. (2019). Evaluation of thermal climatic region areas in terms of building density in urban management and planning for Burdur, Turkey. *Air Quality, Atmosphere and Health*, 12(9), 1103–1112. <https://doi.org/10.1007/s11869-019-00727-3>
- Cetin, M., Adiguzel, F., Kaya, O., & Sahap, A. (2018). Mapping of bioclimatic comfort for potential planning using GIS in Aydin. *Environment, Development and Sustainability*, 20(1), 361–375. <https://doi.org/10.1007/s10668-016-9885-5>
- Chen, F., & Dudhia, J. (2001). Coupling and advanced land surface-hydrology model with the Penn State-NCAR MM5 modeling system. Part I: Model implementation

- and sensitivity. *Monthly Weather Review*, 129(4), 569–585. [https://doi.org/10.1175/1520-0493\(2001\)129\(0569:CAALSH\)2.0.CO;2](https://doi.org/10.1175/1520-0493(2001)129(0569:CAALSH)2.0.CO;2)
- Chen, F., Kusaka, H., Tewari, M., Bao, J. W., & Hirakuchi, H. (2004). Utilizing the coupled WRF/LSM/urban modeling system with detailed urban classification to simulate the urban heat island phenomena over the Greater Houston area. *5th Symposium on the Urban Environment*, 431–437.
- Chen, F., Kusaka, H., Bornstein, R., Ching, J., Grimmond, C. S. B., Grossman-Clarke, S., Loridan, T., Manning, K. W., Martilli, A., Miao, S., Sailor, D., Salamanca, F. P., Taha, H., Tewari, M., Wang, X., Wyszogrodzki, A. A., & Zhang, C. (2011a). The integrated WRF/urban modelling system: Development, evaluation, and applications to urban environmental problems. *International Journal of Climatology*, 31(2), 273–288. <https://doi.org/10.1002/joc.2158>
- Chen, Q., Yuan, Y., Huang, X., He, Z., & Tan, H. (2018). Assessment of column aerosol optical properties using ground-based sun-photometer at urban Harbin, Northeast China. *Journal of Environmental Sciences (china)*, 74(2017), 50–57. <https://doi.org/10.1016/j.jes.2018.02.003>
- Chen, Y., Yang, K., He, J., Qin, J., Shi, J., Du, J., & He, Q. (2011b). Improving land surface temperature modeling for dry land of China. *Journal of Geophysical Research*, 116, 20104. <https://doi.org/10.1029/2011JD015921>
- Cheng, F. Y., Hsu, Y. C., Lin, P. L., & Lin, T. H. (2013). Investigation of the effects of different land use and land cover patterns on mesoscale meteorological simulations in the Taiwan area. *Journal of Applied Meteorology and Climatology*, 52(3), 570–587. <https://doi.org/10.1175/JAMC-D-12-0109.1>
- Friedl, M. A., McIver, D. K., Hodges, J. C. F., Zhang, X. Y., Muchoney, D., Strahler, A. H., Woodcock, C. E., Gopal, S., Schneider, A., Cooper, A., Baccini, A., Gao, F., & Schaaf, C. (2002). Global land cover mapping from MODIS: Algorithms and early results. *Remote Sensing of Environment*, 83(1–2), 287–302. [https://doi.org/10.1016/S0034-4257\(02\)00078-0](https://doi.org/10.1016/S0034-4257(02)00078-0)
- Friedl, M. A., Sulla-Menashe, D., Tan, B., Schneider, A., Ramankutty, N., Sibley, A., & Huang, X. (2010). MODIS Collection 5 global land cover: Algorithm refinements and characterization of new datasets. *Remote Sensing of Environment*, 114(1), 168–182. <https://doi.org/10.1016/j.rse.2009.08.016>
- Fu, D., Shi, X., Xing, Y., Wang, P., Li, H., Li, B., Lu, L., Thapa, S., Yabo, S., Qi, H., & Zhang, W. (2021a). Contributions of extremely unfavorable meteorology and coal-heating boiler control to air quality in December 2019 over Harbin, China. *Atmospheric Pollution Research*, 12(11), 1–10. <https://doi.org/10.1016/j.apr.2021.101217>
- Fu, D., Zhang, W., Xing, Y., Li, H., Wang, P., Li, B., Shi, X., Zuo, J., Yabo, S., Thapa, S., Lu, L., Qi, H., & Ma, J. (2021b). Impacts of maximum snow albedo and land cover changes on meteorological variables during winter in northeast China. *Atmospheric Research*, 254, 105449. <https://doi.org/10.1016/j.atmosres.2021.105449>
- Gedzelman, S. D., Austin, S., Cermak, R., Stefano, N., Partridge, S., Quesenberry, S., & Robinson, D. A. (2003). Mesoscale aspects of the Urban Heat Island around New York City. *Theoretical and Applied Climatology*, 75(1–2), 29–42. <https://doi.org/10.1007/s00704-002-0724-2>
- Georgescu, M. (2015). Challenges associated with adaptation to future urban expansion. *Journal of Climate*, 28(7), 2544–2563. <https://doi.org/10.1175/JCLI-D-14-00290.1>
- Ghadban, M., Baayoun, A., Lakkis, I., Najem, S., Saliba, N. A., & Shihadeh, A. (2020). A novel method to improve temperature forecast in data-scarce urban environments with application to the Urban Heat Island in Beirut. *Urban Climate*, 33(March), 100648. <https://doi.org/10.1016/j.uclim.2020.100648>
- Giannaros, C., Nenes, A., Giannaros, T. M., Kourtidis, K., & Melas, D. (2018). A comprehensive approach for the simulation of the Urban Heat Island effect with the WRF/SLUCM modeling system: The case of Athens (Greece). *Atmospheric Research*, 201, 86–101. <https://doi.org/10.1016/j.atmosres.2017.10.015>
- Giannaros, T. M., Melas, D., Daglis, I. A., Keramitsoglou, I., & Kourtidis, K. (2013). Numerical study of the urban heat island over Athens (Greece) with the WRF model. *Atmospheric Environment*, 73, 103–111. <https://doi.org/10.1016/j.atmosenv.2013.02.055>
- Göndöcs, J., Breuer, H., Pongrácz, R., & Bartholy, J. (2017). Urban heat island mesoscale modelling study for the Budapest agglomeration area using the WRF model. *Urban Climate*, 21, 66–86. <https://doi.org/10.1016/j.uclim.2017.05.005>
- Gong, P. (2009). Accuracy test on global land cover map based on the global flux observation station. *Progress in Natural Science*, 19(7), 754–759.
- Gungor, S., Cetin, M., & Adiguzel, F. (2021). Calculation of comfortable thermal conditions for Mersin urban city planning in Turkey. *Air Quality, Atmosphere and Health*, 14(4), 515–522. <https://doi.org/10.1007/s11869-020-00955-y>
- He, C., Zhou, L., Yao, Y., Ma, W., & Kinney, P. L. (2020). Estimating spatial effects of anthropogenic heat emissions upon the urban thermal environment in an urban agglomeration area in East China. *Sustainable Cities and Society*, 57, 102046. <https://doi.org/10.1016/j.scs.2020.102046>
- Holec, J., Feranec, J., Šťastný, P., Szatmári, D., Kopecák, M., & Garaj, M. (2020). Evolution and assessment of urban heat island between the years 1998 and 2016: Case study of the cities Bratislava and Trnava in western Slovakia. *Theoretical and Applied Climatology*, 141(3–4), 979–997. <https://doi.org/10.1007/s00704-020-03197-1>
- Huang, D., & Gao, S. (2018). Impact of different reanalysis data on WRF dynamical downscaling over China. *Atmospheric Research*, 200, 25–35. <https://doi.org/10.1016/j.atmosres.2017.09.017>
- Huang, M., Cui, P., & He, X. (2018). Study of the cooling effects of urban green space in Harbin in terms of reducing the heat island effect. *Sustainability (switzerland)*, 10(4), 1–17. <https://doi.org/10.3390/su10041101>
- Huang, Q., & Lu, Y. (2015). The effect of urban heat island on climate warming in the Yangtze River Delta urban agglomeration in China. *International Journal of Environmental Research and Public Health*, 12(8), 8773–8789. <https://doi.org/10.3390/ijerph120808773>
- Huidong, L. (2018). *Urban heat island and its influencing mechanism in the city of Berlin*.

- Ichinose, T., Shimodozo, K., & Hanaki, K. (1999). Impact of anthropogenic heat on urban climate in Tokyo. *Atmospheric Environment*, 33(24–25), 3897–3909. [https://doi.org/10.1016/S1352-2310\(99\)00132-6](https://doi.org/10.1016/S1352-2310(99)00132-6)
- Jain, S., Roy, S. B., Panda, J., & Rath, S. S. (2021). Modeling of land-use and land-cover change impact on summertime near-surface temperature variability over the Delhi-Mumbai Industrial Corridor. *Modeling Earth Systems and Environment*, 7(2), 1309–1319. <https://doi.org/10.1007/s40808-020-00959-8>
- Jandaghian, Z., & Berardi, U. (2020). Comparing urban canopy models for microclimate simulations in Weather Research and Forecasting Models. *Sustainable Cities and Society*, 55, 102025. <https://doi.org/10.1016/j.scs.2020.102025>
- Javadinejad, S., Eslamian, S., & Ostad-Ali-Askari, K. (2021). The analysis of the most important climatic parameters affecting performance of crop variability in a changing climate. *International Journal of Hydrology Science and Technology*, 11(1), 1–25. <https://doi.org/10.1504/IJHST.2021.112651>
- Jihong, L., Weifeng, Z., Wenqu, C., Yongqi, L., Yifan, X., & Fan, Z. (2020). 基于 RS 的哈尔滨市土地利用变化对碳储量的影响. *Influence of Land Use on Carbon Storage Based on RS in Harbin*. 34(2). <https://doi.org/10.16270/j.cnki.slgc.2018.02.001>
- José, R. S., Pérez, J. L., & González, R. M. (2013). Using WRF/UCM and CMAQ mesoscale models with very high resolution over European urban cities. *Fresenius Environmental Bulletin*, 22(12 C), 3815–3822. <https://doi.org/10.1007/978-94-007-7756-9>
- Kim, G., Lee, J., Lee, M. I., & Kim, D. (2021). Impacts of urbanization on atmospheric circulation and aerosol transport in a coastal environment simulated by the WRF-Chem coupled with urban canopy model. In *Atmospheric Environment*, 249. <https://doi.org/10.1016/j.atmosenv.2021.118253>
- Kirthiga, S. M., & Patel, N. R. (2018). Impact of updating land surface data on micrometeorological weather simulations from the WRF model. *Atmosfera*, 31(2), 165–183. <https://doi.org/10.20937/ATM.2018.31.02.05>
- Kusaka, H., Chen, F., Tewari, M., & Hirakuchi, H. (2005). Impact of using the urban canopy model WRF / MM5 Users' Workshop - June 2005 WRF / MM5 Users' Workshop - June 2005. *Sixth symposium on the urban environment AMS forum: Managing our physical and natural resources: Successes and challenges*, 5–8.
- Li, D., & Bou-Zeid, E. (2014). Quality and sensitivity of high-resolution numerical simulation of urban heat islands. *Environmental Research Letters*, 9(5). <https://doi.org/10.1088/1748-9326/9/5/055001>
- Li, D., Bou-Zeid, E., Barlage, M., Chen, F., & Smith, J. A. (2013). Development and evaluation of a mosaic approach in the WRF-Noah framework. *Journal of Geophysical Research Atmospheres*, 118(21), 11918–11935. <https://doi.org/10.1002/2013JD020657>
- Li, H., Meier, F., Lee, X., Chakraborty, T., Liu, J., Schaap, M., & Sodoudi, S. (2018a). Interaction between urban heat island and urban pollution island during summer in Berlin. *Science of the Total Environment*, 636, 818–828. <https://doi.org/10.1016/j.scitotenv.2018.04.254>
- Li, H., Wolter, M., Wang, X., & Sodoudi, S. (2018b). Impact of land cover data on the simulation of urban heat island for Berlin using WRF coupled with bulk approach of Noah-LSM. *Theoretical and Applied Climatology*, 134(1–2), 67–81. <https://doi.org/10.1007/s00704-017-2253-z>
- Li, H., Zhou, Y., Wang, X., Zhou, X., Zhang, H., & Sodoudi, S. (2019). Quantifying urban heat island intensity and its physical mechanism using WRF/UCM. *Science of the Total Environment*, 650, 3110–3119. <https://doi.org/10.1016/j.scitotenv.2018.10.025>
- Li, H., Zhang, H., Mamtimin, A., Fan, S., & Ju, C. (2020). A new land-use dataset for the weather research and forecasting (WRF) model. April 1992.
- Liu, T., Zhang, S., Yu, L., Bu, K., Yang, J., & Chang, L. (2017). Simulation of regional temperature change effect of land cover change in agroforestry ecotone of Nenjiang River Basin in China. *Theoretical and Applied Climatology*, 128(3–4), 971–981. <https://doi.org/10.1007/s00704-016-1750-9>
- Liu, Y., Li, Q., Yang, L., Mu, K., Zhang, M., & Liu, J. (2020). Urban heat island effects of various urban morphologies under regional climate conditions. *Science of the Total Environment*. <https://doi.org/10.1016/j.scitotenv.2020.140589>
- Loveland, T. R., Merchant, J. W., Brown, J. F., Ohlen, D., Reed, B. C., Olson, P., & Hutchinson, J. (1995). *Map Supplement*, 85(2), 339–355.
- Mahmood, R., Pielke, R. A., Hubbard, K. G., Niyogi, D., Dirmeyer, P. A., Mcalpine, C., Carleton, A. M., Hale, R., Gameda, S., Beltrán-Przekurat, A., Baker, B., Mcnider, R., Legates, D. R., Shepherd, M., Du, J., Blanken, P. D., Frauenfeld, O. W., Nair, U. S., & Fall, S. (2014). Land cover changes and their biogeophysical effects on climate. *International Journal of Climatology*, 34(4), 929–953. <https://doi.org/10.1002/joc.3736>
- Massad, R. S., Lathiére, J., Strada, S., Perrin, M., Personne, E., Stéfanon, M., Stella, P., Szopa, S., & De Noblet-Ducoudré, N. (2019). Reviews and syntheses: Influences of landscape structure and land uses on local to regional climate and air quality. *Biogeosciences*, 16(11), 2369–2408. <https://doi.org/10.5194/bg-16-2369-2019>
- Mirzaei, P. A., & Haghhighat, F. (2010). Approaches to study Urban Heat Island – Abilities and limitations. *Building and Environment*, 45(10), 2192–2201. <https://doi.org/10.1016/j.buildenv.2010.04.001>
- Mughal, M. O., Li, X. X., & Norford, L. K. (2020). Urban heat island mitigation in Singapore: Evaluation using WRF/multilayer urban canopy model and local climate zones. *Urban Climate*, 34(October), 100714. <https://doi.org/10.1016/j.uclim.2020.100714>
- Myrup, L. O. (1969). A numerical model of the urban heat island. *Journal of Applied Meteorology and Climatology*, 8, 908–918.
- Neethu, C., & Ramesh, K. V. (2022). High-resolution spatiotemporal variability of heat wave impacts quantified by thermal indices. *Theoretical and Applied Climatology*, 1995(0123456789). <https://doi.org/10.1007/s00704-022-03987-9>
- Oke, T. R. (1982). The energetic basis of the urban heat island. *Quarterly Journal of the Royal Meteorological Society*, 108(455), 1–24. <https://doi.org/10.1002/qj.49710845502>

- Oke, T. R. (1988). The urban energy balance. *Progress in Physical Geography*, 12(4), 471–508. <https://doi.org/10.1177/03091338801200401>
- Oke, T. R. (1995). The Heat Island of the urban boundary layer: Characteristics, causes and effects. *Wind Climate in Cities*, 1, 81–107. https://doi.org/10.1007/978-94-017-3686-2_5
- Ostad-Ali-Askari, K., Su, R., & Liu, L. (2018). Editorial: Water resources and climate change. *Journal of Water and Climate Change*, 9(2), 239. <https://doi.org/10.2166/wcc.2018.999>
- Palou, F. S., & Mahalov, A. (2019). Summer- and wintertime variations of the surface and near-surface urban heat island in a semiarid environment. *Weather and Forecasting*, 34(6), 1849–1865. <https://doi.org/10.1175/WAF-D-19-0054.1>
- Porangaba, G. F. O., Teixeira, D. C. F., Amorim, M. C. D. C. T., Da Silva, M. H. S., & Dubreuil, V. (2021). Modeling the urban heat island at a winter event in Três Lagoas, Brazil. *Urban Climate*, 37(February), 100853. <https://doi.org/10.1016/j.uclim.2021.100853>
- Rizwan, A. M., Dennis, L. Y. C., & Liu, C. (2008). A review on the generation, determination and mitigation of Urban Heat Island. *Journal of Environmental Sciences*, 20(1), 120–128. [https://doi.org/10.1016/S1001-0742\(08\)60019-4](https://doi.org/10.1016/S1001-0742(08)60019-4)
- Salamanca, F., Georgescu, M., Mahalov, A., & Moustaoui, M. (2015). Summertime response of temperature and cooling energy demand to urban expansion in a semiarid environment. *Journal of Applied Meteorology and Climatology*, 54(8), 1756–1772. <https://doi.org/10.1175/JAMC-D-14-0313.1>
- Sellers, P. J., Dickinson, R. E., Randall, D. A., Betts, A. K., Hall, F. G., Berry, J. A., Collatz, G. J., Denning, A. S., Mooney, H. A., Nobre, C. A., Sato, N., Field, C. B., & Henderson-Sellers, A. (1997). Modeling the exchanges of energy, water, and carbon between continents and the atmosphere. *Science*, 275(5299), 502–509. <https://doi.org/10.1126/science.275.5299.502>
- Sertel, E., Robock, A., & Ormeci, C. (2010). Impacts of land cover data quality on regional climate simulations. *International Journal of Climatology*, 30(13), 1942–1953. <https://doi.org/10.1002/joc.2036>
- Shahmohamadi, P., Che-Ani, A. I., Maulud, K. N. A., Tawil, N. M., & Abdullah, N. A. G. (2011). The Impact of anthropogenic heat on formation of Urban Heat Island and energy consumption balance. *Urban Studies Research*, 2011, 1–9. <https://doi.org/10.1155/2011/497524>
- Sun, J., & Mahrt, L. (1995). Relationship of surface heat flux to microscale temperature variations: Application to boreas. *Boundary-Layer Meteorology*, 76(3), 291–301. <https://doi.org/10.1007/BF00709355>
- Sun, X., Wang, K., Li, B., Zong, Z., Shi, X., Ma, L., Fu, D., Thapa, S., Qi, H., & Tian, C. (2020). Exploring the cause of PM_{2.5} pollution episodes in a cold metropolis in China. *Journal of Cleaner Production*, 256. <https://doi.org/10.1016/j.jclepro.2020.120275>
- Talebmorad, H., Abedi-Koupai, J., Eslamian, S., Mousavi, S. F., Akhavan, S., Ostad-Ali-Askari, K., & Singh, V. P. (2021). Evaluation of the impact of climate change on reference crop evapotranspiration in Hamedan-Bahar plain. *International Journal of Hydrology Science and Technology*, 11(3), 333–347. <https://doi.org/10.1504/IJHST.2021.114554>
- Taylor, K. E. (2001). Summarizing multiple aspects of model performance in a single diagram. *Journal of Geophysical Research: Atmospheres*, 106(D7), 7183–7192. <http://dx.doi.org/10.1029/2000JD900719>
- Tewari, M., Salamanca, F., Martilli, A., Treinish, L., & Mahalov, A. (2017). Impacts of projected urban expansion and global warming on cooling energy demand over a semiarid region. *Atmospheric Science Letters*, 18(11), 419–426. <https://doi.org/10.1002/asl.784>
- Tewari, M., Yang, J., Kusaka, H., Salamanca, F., Watson, C., & Treinish, L. (2019). Interaction of urban heat islands and heat waves under current and future climate conditions and their mitigation using green and cool roofs in New York City and Phoenix, Arizona. *Environmental Research Letters*, 14(3). <https://doi.org/10.1088/1748-9326/aaf431>
- Vogel, J., & Afshari, A. (2020). Comparison of urban heat island intensity estimation methods using urbanized WRF in Berlin, Germany. *Atmosphere*, 11(12). <https://doi.org/10.3390/atmos11121338>
- Wang, L., & Li, D. (2021). Urban heat islands during heat waves: A comparative study between Boston and Phoenix. *Journal of Applied Meteorology and Climatology*, 60(5), 621–641. <https://doi.org/10.1175/JAMC-D-20-0132.1>
- Wang, Q., Zhang, C., Ren, C., Hang, J., & Li, Y. (2020). Urban heat island circulations over the Beijing-Tianjin region under calm and fair conditions. *Building and Environment*, 180, 107063. <https://doi.org/10.1016/j.buildenv.2020.107063>
- Wang, S., & Sun, B. (2017). The impacts of different land surface parameterization schemes on Northeast China snowfall simulation. *Meteorology and Atmospheric Physics*. <https://doi.org/10.1007/s00703-017-0539-4>
- Wang, S., & Sun, B. (2018). The impacts of different land surface parameterization schemes on Northeast China snowfall simulation. *Meteorology and Atmospheric Physics*, 130(5), 583–590. <https://doi.org/10.1007/s00703-017-0539-4>
- Wang, Z., Song, K., Ma, W., Ren, C., Zhang, B., Liu, D., Chen, J. M., & Song, C. (2011). Loss and fragmentation of marshes in the sanjiang plain, Northeast China, 1954–2005. *Wetlands*, 31(5), 945–954. <https://doi.org/10.1007/s13157-011-0209-0>
- Xiaolin, C. (2017). The analysis of land use change and its driving forces in Harbin City Cheng. *Natural Sciences Journal of Harbin Normal University*, 33(6). <http://www.cnki.net>
- Yang, B., Zhang, Y., & Qian, Y. (2012). Simulation of urban climate with high-resolution WRF model: A case study in Nanjing, China. *Asia-Pacific Journal of Atmospheric Sciences*, 48(3), 227–241. <https://doi.org/10.1007/s13143-012-0023-5>
- Yang, C., He, X., Yu, L., Yang, J., Yan, F., Bu, K., Chang, L., & Zhang, S. (2017a). The cooling effect of urban parks and its monthly variations in a snow climate city. *Remote Sensing*, 9(10). <https://doi.org/10.3390/rs9101066>
- Yang, Y., Xiao, P., Feng, X., & Li, H. (2017b). Accuracy assessment of seven global land cover datasets over China. *ISPRS Journal of Photogrammetry and Remote Sensing*, 125, 156–173. <https://doi.org/10.1016/j.isprsjprs.2017.01.016>
- Zeren Cetin, I., Ozel, H. B., & Varol, T. (2020). Integrating of settlement area in urban and forest area of Bartin with climatic condition decision for managements. *Air Quality*,

- Atmosphere and Health*, 13(8), 1013–1022. <https://doi.org/10.1007/s11869-020-00871-1>
- Zeren Cetin, I., & Sevik, H. (2020). Investigation of the relationship between bioclimatic comfort and land use by using GIS and RS techniques in Trabzon. In *Environmental Monitoring and Assessment* (Vol. 192, Issue 2). <https://doi.org/10.1007/s10661-019-8029-4>
- Zhang, X., Steeneveld, G. J., Zhou, D., Ronda, R. J., Duan, C., Koopmans, S., & Holtslag, A. A. M. (2020). Modelling urban meteorology with increasing refinements for the complex morphology of a typical Chinese city (Xi'an). *Building and Environment*, 182(99), 107109. <https://doi.org/10.1016/j.buildenv.2020.107109>
- Zhao, H., Tong, D. Q., Gao, C., & Wang, G. (2015). Effect of dramatic land use change on gaseous pollutant emissions from biomass burning in Northeastern China. *Atmospheric Research*, 153, 429–436. <https://doi.org/10.1016/j.atmosres.2014.10.008>
- Zhao, Z. Q., He, B. J., Li, L. G., Wang, H. B., & Darko, A. (2017). Profile and concentric zonal analysis of relationships between land use/land cover and land surface temperature: Case study of Shenyang, China. *Energy and Buildings*, 155, 282–295. <https://doi.org/10.1016/j.enbuild.2017.09.046>
- Zhong, S., Qian, Y., Zhao, C., Leung, R., Wang, H., Yang, B., Fan, J., Yan, H., Yang, X. Q., & Liu, D. (2017). Urbanization-induced urban heat island and aerosol effects on climate extremes in the Yangtze River Delta region of China. *Atmospheric Chemistry and Physics*, 17(8), 5439–5457. <https://doi.org/10.5194/acp-17-5439-2017>
- Zhou, X., & Chen, H. (2018). Impact of urbanization-related land use land cover changes and urban morphology changes on the urban heat island phenomenon. *Science of the Total Environment*, 635, 1467–1476. <https://doi.org/10.1016/j.scitotenv.2018.04.091>
- Zhou, Y., & Shepherd, J. M. (2010). Atlanta's urban heat island under extreme heat conditions and potential mitigation strategies. *Natural Hazards*, 52(3), 639–668. <https://doi.org/10.1007/s11069-009-9406-z>

Publisher's note Springer Nature remains neutral with regard to jurisdictional claims in published maps and institutional affiliations.